

# Domain Formation and Permeabilization Induced by the Saponin $\alpha$ -Hederin and Its Aglycone Hederagenin in a Cholesterol-Containing Bilayer

Joseph Lorent,<sup>†,‡</sup> Laurence Lins,<sup>§</sup> Òscar Domenech,<sup>||</sup> Joelle Quetin-Leclercq,<sup>‡</sup> Robert Brasseur,<sup>§</sup> and Marie-Paule Mingeot-Leclercq<sup>\*,†</sup>

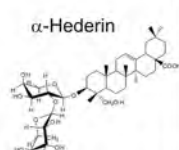
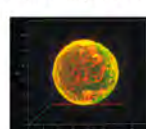

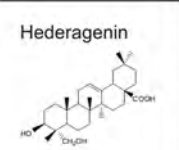
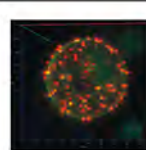
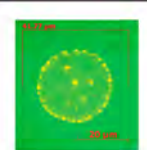
<sup>†</sup>Université Catholique de Louvain, Louvain Drug Research Institute, Cellular and Molecular Pharmacology, B1.73.05, Avenue E. Mounier 73, B-1200 Brussels, Belgium

<sup>‡</sup>Université Catholique de Louvain, Louvain Drug Research Institute, Pharmacognosy, B1.72.03, Avenue E. Mounier 72, B-1200 Brussels, Belgium

<sup>§</sup>ULg, Centre de Biophysique Moléculaire Numérique, Agro-BioTech Gembloux, Passage des Déportés, 2, B-5030 Gembloux, Belgium

<sup>||</sup>University of Barcelona, Departament de Fisicoquímica, Facultat de Farmàcia, UB and Institut de Nanociència i Nanotecnologia IN, 08028 Barcelona, Spain

## Supporting Information

	Concentration / Time	Phase separation	Permeabilization	Aggregation
 $\alpha$ -Hederin	< CMC / 2h			Sterols, phospholipids
 Hederagenin	> CMC / 48h			Phospholipids

**ABSTRACT:** Saponins and triterpenic acids have been shown to be able to interact with lipid membranes and domains enriched with cholesterol (rafts). How saponins are able to modulate lipid phase separation in membranes and the role of the sugar chains for this activity is unknown. We demonstrate in a binary membrane model composed of DMPC/Chol (3:1 mol/mol) that the saponin  $\alpha$ -hederin and its aglycone presenting no sugar chain, the triterpenic acid hederagenin, are able to induce the formation of lipid domains. We show on multilamellar vesicles (MLV), giant unilamellar vesicles (GUV), and supported planar bilayers (SPB) that the presence of sugar units on the saponin accelerates domain formation and increases the proportion of sterols within these domains. The domain shape is also influenced by the presence of sugars because  $\alpha$ -hederin and hederagenin induce the formation of tubular and spherical domains, respectively. These highly curved structures should result from the induction of membrane curvature by both compounds. In addition to the formation of domains,  $\alpha$ -hederin and hederagenin permeabilize GUV. The formation of membrane holes by  $\alpha$ -hederin comes along with the accumulation of lipids into nonbilayer structures in SPB. This process might be responsible for the permeabilizing activity of both compounds. In LUV, permeabilization by  $\alpha$ -hederin was sterol-dependent. The biological implications of our results and the mechanisms involved are discussed in relation to the activity of saponins and triterpenic acids on membrane rafts, cancer cells, and hemolysis.

## INTRODUCTION

Lipid phase separation has become an important concept in membrane organization and has been associated with the formation of lateral functional domains in cells, also called lipid rafts. Rafts are temporary domains having a nanoscopic size of about 10–200 nm. Their fusion into larger domains would provide platforms for protein signaling. Cholesterol is an essential component of these lipid rafts.<sup>1</sup> Because of its rigid planar steroid ring system, it induces a high conformational order

of the lipid acyl chains. This results in a condensing effect with a decrease in the area occupied by the other lipids as well as an increase in the bilayer thickness. It also modifies the thermotropic phase transition between the liquid-disordered phase, often termed the fluid phase ( $L_d$  or  $L_\alpha$ ), and the solid-

Received: June 20, 2013

Revised: February 19, 2014

ordered phase, also called the gel phase ( $S_0$ ), by inducing an intermediate liquid-ordered ( $L_0$  or  $L_\beta$ ) phase.<sup>2</sup> In model membranes, the  $L_0$  phase is laterally separated from the  $L_d$  phase and is thought to mimic lipid rafts in cells.

In addition to lamellar bilayer phases, nonlamellar lipid mesophases (hexagonal, cubic, and isotropic) can be present in biological membranes, and some of these nonbilayer phases are thought to be important for protein/membrane interactions and fusion.<sup>3,4</sup> Besides their biological function, nonlamellar phases can be induced when amphiphilic drugs or peptides come into contact with membranes. The formation of the normal isotropic or hexagonal ( $H_I$ ) phase has also been put in relationship with the permeabilization of membranes.<sup>5</sup> At intermediate amphiphiles/phospholipids ratios, the bilayer phase can coexist with the newly formed phase.<sup>6</sup> Sometimes, even macroscopic phase separation becomes visible in the sample.<sup>7</sup>

Several saponins, amphiphilic compounds of natural origin, are known for their ability to interact with membrane rafts and especially with cholesterol, the major component of rafts.<sup>8,9</sup> Among them are avicin D, ginsenoside Rh2, and glycyrrhizin which in parallel alter membrane permeability.<sup>9–11</sup> Some triterpenic acids, lacking the sugar chains of saponins, have also shown the potential to interact with rafts.<sup>12</sup> Recently, we reported  $\alpha$ -hederin-induced cholesterol-dependent permeabilization and the formation of toroidal pores, assuming saponin/cholesterol-enriched domains with increased transbilayer curvature in the bilayer.<sup>13</sup> The induction of curvature by  $\alpha$ -hederin and hederagenin, its triterpenic aglycone, was correlated to the formation of a highly curved lipid mesophase.<sup>13</sup> Similar effects were observed with other saponins, namely, glycoalkaloids<sup>14</sup> and digitonin.<sup>15</sup> The formation of a new lipid phase with the saponin depended upon the interaction of the compound with cholesterol and the presence of the sugar chain at C3 on the aglycone.<sup>13,14</sup>

Understanding the mechanisms that drive interactions with lipid rafts, the formation of lateral domains, the transformation of the bilayer into nonlamellar structures, and the permeabilization of the membrane by saponins are essential to explaining their biological effects.

For this purpose, we investigated the ability of  $\alpha$ -hederin (hederagenin 3-*O*- $\alpha$ -L-rhamnopyranosyl-(1  $\rightarrow$  2)- $\alpha$ -L-arabinopyranoside) and hederagenin, with its aglycone lacking the sugar chain, to induce domain formation in a dimyristoylphosphatidylcholine (DMPC)/cholesterol (chol) (3:1) model. This simplistic binary membrane model has the advantage of presenting a nanoscopic  $L_0$  phase enriched in cholesterol at ambient temperature. This is similar to what has been observed for lipid rafts in cells even if the lipid composition in biological membranes is much more complex.<sup>13,16–19</sup> The same binary model has also been used to show domain formation induced by glycoalkaloids in monolayers<sup>20</sup> and to investigate the mechanism of permeabilization induced by  $\alpha$ -hederin,<sup>13</sup> which facilitated comparison with other published results.

We selected complementary investigation techniques to understand the membrane activity of  $\alpha$ -hederin and hederagenin. By molecular modeling and fluorescence spectroscopy of dehydroergosterol (DHE), a fluorescent cholesterol analogue,<sup>21</sup> we demonstrated the ability of  $\alpha$ -hederin and hederagenin to interact with sterols. Using Förster resonance energy transfer (FRET) of DHE and diphenylhexatriene-phosphatidylcholine (DPH-PC) inserted into multilamellar vesicles (MLVs), we monitored the quantitative and temporal aspects of lipid phase separation. Using giant unilamellar vesicles (GUVs), we

visualized by fluorescence and confocal microscopy using Texas red dipalmitoylphosphoethanolamine (TR-DPPE) and 2-dipalmitoyl-*sn*-glycero-3-phosphoethanolamine-*N*-7-nitro-2-1,3-benzoxadiazol-4-yl (NBD-DPPE) the ability of  $\alpha$ -hederin and hederagenin to induce lateral domains.<sup>22</sup> To investigate the relationship of the permeabilizing and domain-forming activity, we tested the permeation of GUVs to dextran-FITC. We further characterized the importance of sterols regarding domain formation and permeabilization by using two-photon microscopy of DHE<sup>23</sup> and calcein release from LUVs, respectively. In parallel, we determined the effect of  $\alpha$ -hederin on supported planar bilayers (SPBs) by atomic force microscopy (AFM) to gain insight into the nanoscopic aspects of domain formation and permeabilization.

This study shows how  $\alpha$ -hederin and hederagenin are able to promote the formation of microscopical domains. It gives some insights on how a saponin and a triterpenic acid could be able to interact with lipid rafts in cellular membranes and induce membrane permeabilization.

## MATERIAL AND METHODS

**Material.**  $\alpha$ -Hederin and hederagenin (HPLC quality) were purchased from Extrasynthese, (Genay, France) and dissolved in ethanol. After the evaporation of the solvent, the residue was dissolved in buffer solution (10 mM Tris-HCl adjusted to pH 7.4 with NaOH) containing 0.1% DMSO to prevent solubility problems. DMPC (dimyristoyl-*sn*-glycero-3-phosphocholine) and cholesterol were purchased from Avanti Polar Lipids. TR-DPPE (Texas red 1,2-dipalmitoyl-*sn*-glycero-3-phosphoethanolamine), NBD-DPPE (*N*-(7-nitrobenz-2-oxa-1,3-diazol-4-yl)-1,2-dihexadecanoyl-*sn*-glycero-3-phosphoethanolamine), DPH-PC (diphenylhexatriene phosphatidylcholine), and R18 (octadecylrhodamine) were purchased from Invitrogen (Paisley, Scotland, U.K.). DHE (dehydroergosterol), calcein, stigmasterol, and FITC-dextran (4 kDa) were purchased from Sigma-Aldrich (St. Louis, MO). PDMS (poly(dimethylsiloxane)) was kindly provided by Henri Burhin and Christian Bailly (SST/Institute of Condensed Matter and Nanosciences, Bio and Soft Matter, Université Catholique de Louvain, Louvain-la-Neuve). Ergosterol was purchased from Fluka Chemika (Lyon, France), and all other reagents were from E. Merck AG (Darmstadt, Germany).

**Dehydroergosterol (DHE) Spectroscopy to Investigate Interactions with Sterols in Aqueous Solution.** Spectral features of DHE give insights into the ratio between monomers and the aggregated form<sup>24</sup> as well as the microenvironment of DHE in aqueous solution.<sup>25,26</sup> When DHE is excited at 310 nm in aqueous solution, the ratio between the fluorescence intensities at 375 versus 395 or 424 nm ( $I_{375}/I_{395}$  or  $I_{375}/I_{424}$ ) reflects the ratio of monomers versus microcrystals in aqueous solution.<sup>24</sup> Moreover, a decrease in the dielectric constant of the microenvironment of DHE induces a blue shift in  $\lambda_{\max}$  emission.<sup>25</sup>

The aqueous dispersions of DHE (10  $\mu$ M) were prepared as previously described to obtain DHE in a final solution of 10 mM Tris-HCl at pH 7.4 containing 0.1% DMSO.<sup>13</sup> Fluorescence emission spectra of DHE in buffer solution were taken at increasing concentrations of  $\alpha$ -hederin and hederagenin, and the intensity of the monomeric versus microcrystalline peak ratio was plotted against  $\log_{10}$  concentration. The influence of DMSO and DHE concentration was checked. The excitation monochromator was set to 310 nm (slit = 4.5), and the emission spectra were recorded from 335 to 445 nm.<sup>25,26</sup>

**Molecular Modeling and Assembly of  $\alpha$ -Hederin and Hederagenin with Lipids.** The assembly of  $\alpha$ -hederin or hederagenin with DMPC or cholesterol was studied by molecular modeling. The method was derived from the hypermatrix method described elsewhere.<sup>27</sup> The molecules ( $\alpha$ -hederin, hederagenin, cholesterol, and DMPC) were first oriented at the interface, taking their hydrophobic and hydrophilic centers into account.<sup>28</sup> For each pair of molecules ( $\alpha$ -hederin/ $\alpha$ -hederin,  $\alpha$ -hederin/Chol,  $\alpha$ -hederin/DMPC, hederagenin/hederagenin, hederagenin/Chol, and hederagenin/DMPC), the inter-

action energies (sum of electrostatic, van der Waals, and hydrophobic energies) were calculated for more than  $10^7$  positions.<sup>29</sup> This interaction energy matrix was also used in the big layer method described in the Supporting Information.

**Steady-State Fluorescence Measurements on MLVs to Investigate Phase Separation.** Fluorescence spectra and intensity measurements of MLV were performed on a LS55 luminescence spectrometer (PerkinElmer Ltd., Beaconsfield, U.K.). Temperature was controlled with a Phoenix II C25P bath (Thermo Fisher Scientific, Waltham, MA). FRET measurements of DHE and DPH-PC were made on a Spectramax M3 (Molecular Devices, Sunnyvale, CA).

**Preparation of Multilamellar Vesicles (MLVs).** Multilamellar vesicles (MLVs) composed of DMPC/Chol (3:1) were prepared by the freeze–thawing technique. A dry lipid film was formed by evaporating a lipid solution of 10 mg/mL total lipid in  $\text{CHCl}_3/\text{CH}_3\text{OH}$  (2:1 v/v) using a rotavapor R-210 (Buchi Labortechnik AG, Flawil, Switzerland). The film was resuspended in a buffer solution (Tris-HCl 10 mM at pH 7.4). The suspension was submitted to five cycles of freezing/thawing to obtain multilamellar vesicles (MLVs). The lipid concentration of the liposomal suspension was measured by phosphorus quantification<sup>30</sup> and adjusted according to the experimental protocol used.

**Förster Resonance Energy Transfer (FRET) between DHE and DPH-PC.** FRET provides a measure of the average distance between an array of donor and acceptor molecules. The energy transfer between the donor (DHE) and acceptor (DPH-PC) is efficient when the distance between both molecules does not exceed 1–10 nm.<sup>31</sup> If probes DHE (donor) and DPH-PC (acceptor) are partitioned differently between two lipid phases (e.g.,  $L_o$  and  $L_d$  phases), then the FRET efficiency is low.<sup>32</sup> In MLVs composed of DMPC/Chol/DHE/DPH-PC (75:24:1:0.1 mol/mol/mol/mol), the FRET efficiency was determined by exciting DHE at 310 nm (slit = 4 nm) and taking emission intensities at 371 nm (DHE emission peak) and 430 nm (DPH-PC emission peak). The fluorescence intensity ratio ( $I_{430}/I_{371}$ ) was taken as a measure of the energy-transfer efficiency. Use of the intensity ratio largely eliminated the noise introduced by variations in lipid and probe concentrations between samples.

**Microscopy Studies on GUVs to Visualize Lipid Domains.** Domain formation was followed on GUVs. Probes TR-DPPE and NBD-DPPE were used to visualize the potential of  $\alpha$ -hederin (10  $\mu\text{M}$ ) and hederagenin (40  $\mu\text{M}$ ) to induce domain formation, vesiculation, budding, wrinkling, and macroscopic pore formation. TR-DPPE is a fluorescent probe that partitions into the  $L_d$  phase, and NBD-DPPE partitions into the  $L_o$  phase.<sup>22</sup> DHE was used as fluorescent probe to assess the importance of sterols in domain formation.

**Preparation of Giant Unilamellar Vesicles (GUVs).** DMPC/Chol or DMPC/DHE (3:1 mol/mol) giant unilamellar vesicles were prepared by electroformation as described previously.<sup>13,33</sup> Briefly, a lipid film was prepared from 1  $\mu\text{L}$  of a chloroform solution containing 5 mg/mL lipids and 0.1% mol/mol fluorescent probes. This lipid film was hydrated with a sucrose solution of 0.1 M. GUVs were grown in an electroformation chamber by applying a sinusoidal alternating current of 10 Hz and 1 V for 2 h at 60 °C.

**Fluorescence Microscopy.** A fluorescence microscope (Axioskop 40, Carl Zeiss, Jena, Germany) was used to observe GUVs composed of DMPC/Chol (3:1 mol/mol) and labeled with 0.1% mol/mol TR-DPPE and NBD-DPPE. Signals were recorded with a Nikon digital sight DS-5 M (Nikon, Tokyo, Japan). The acquisition software used was NIS-Elements v. 2.10. All observations were made in a sealed observation chamber of 400  $\mu\text{L}$  filled with a sucrose solution of 0.1 M containing  $\alpha$ -hederin or hederagenin at 0.1% DMSO. For incubation with  $\alpha$ -hederin, one GUV was followed for 2 h 40 min. With hederagenin, domain formation was much slower. We therefore showed representative images of GUVs undergoing domain formation after 4 and 48 h. Three independent experiments were performed. Quantification of different features (domain formation, vesiculation, budding, wrinkling, pore formation, and unchanged vesicles) was carried out for a total of 200 vesicles.

**Confocal Microscopy.** Characterization of domain formation by  $\alpha$ -hederin and its aglycone was performed by confocal microscopy on an Axioobserver spinning disk inverted microscope Z.1 (Carl Zeiss, Jena,

Germany). The spinning disk model was a CSU-X1 (Yokogawa Electric Corporation, Tokyo, Japan). We used an EC Plan-Neofluar 40x/1.30 oil DIC M27, an LCI Plan-Neofluar 63x/1.30 Imm Korr DIC M27, or a Plan-Apochromat 100x/1.40 oil DIC M27 objective. Images were recorded with an AxioCamMR3 using Zeiss AxioVision 4.8.2 software. GUVs were incubated in a sealed artificial chamber containing ~150  $\mu\text{L}$  of sucrose solution (0.1 M) and 10  $\mu\text{M}$   $\alpha$ -hederin or 40  $\mu\text{M}$  hederagenin. Those presenting typical stages of domain formation were recorded. TR-DPPE and NBD-DPPE were excited at 561 and 488 nm, and emission was recorded at 617/73 and 520/35 nm, respectively.

**Two-Photon Microscopy.** To obtain insight into the role of sterols in domain formation, we used two-photon microscopy of GUVs composed of DMPC/DHE (3:1) containing 0.1% mol TR-DPPE. DHE has already been visualized in GUVs presenting phase separation, and no quenching was observed even at high DHE concentrations.<sup>23</sup> A Zeiss Axiovert 200M/LSM Meta confocal microscope (Carl Zeiss, Jena, Germany) was used in parallel with a Chameleon infrared laser (Coherent Inc., Santa Clara, CA) set at 690 nm. Magnification was achieved with a C-Apochromat 63x/1.2 water immersion objective. A Nomarski prism was put in the differential interference contrast (DIC) slot of the objective to reduce the photoselection effect of the lipid probes that was due to the linear polarization of the laser.<sup>34,35</sup> Emission was recorded with two band-pass filters set at 427/75 and 595/40 nm to visualize DHE and TR-DPPE fluorescence, respectively.

**Permeability Studies.** Two complementary methods were used to investigate qualitative and quantitative aspects of permeabilization.

**Permeation of Dextran through Membranes of GUVs.** After electroformation, 20  $\mu\text{L}$  of GUVs was added to the artificial chamber (see above) containing, in addition to 10  $\mu\text{M}$   $\alpha$ -hederin or 40  $\mu\text{M}$  hederagenin, 20  $\mu\text{M}$  FITC-dextran (mean molecular weight of 4 kDa). The FITC-dextran was excited at 488 nm, and the emission was recorded with a 520/35 nm emission filter. TR-DPPE was visualized as described in confocal microscopy. The difference in fluorescence intensity between the outside and inside of one GUV reflects the membrane integrity and has been calculated as previously described.<sup>13</sup> We chose GUVs that presented typical features (budding, domains) that developed during incubation.

**Calcein Release from LUVs.** The leakage of entrapped self-quenched calcein from LUVs induced by a permeabilizing agent can be monitored by the fluorescence increase caused by its dilution.<sup>36</sup> To investigate the importance of the sterols in the permeabilizing effect, we included cholesterol, ergosterol, and stigmasterol in the membranes, the major sterols of mammals, fungi, and plants, respectively.<sup>19</sup>

LUVs containing calcein at self-quenching concentration were prepared in 10 mM Tris-HCl adjusted to pH 7.4 and 400 mosm/L from lipid films composed of DMPC/cholesterol, DMPC/stigmasterol, or DMPC/ergosterol (3:1 mol/mol) by the extrusion technique as previously described.<sup>13</sup>

The calcein-filled liposomes (5  $\mu\text{M}$  lipids) were incubated with  $\alpha$ -hederin at 25 °C for increasing time periods. The percentage of released calcein was calculated using the formula  $[(F_t - F_{\text{contr}})/(F_{\text{tot}} - F_{\text{contr}})] \times 100$ .  $F_t$  is the fluorescence signal for a given concentration of  $\alpha$ -hederin and a given incubation period.  $F_{\text{contr}}$  is the fluorescence signal for liposomes without any agent for the same incubation period.  $F_{\text{tot}}$  is the fluorescence signal of liposomes incubated with 2% Triton X-100. The excitation and emission wavelengths were 472 and 512 nm, respectively.

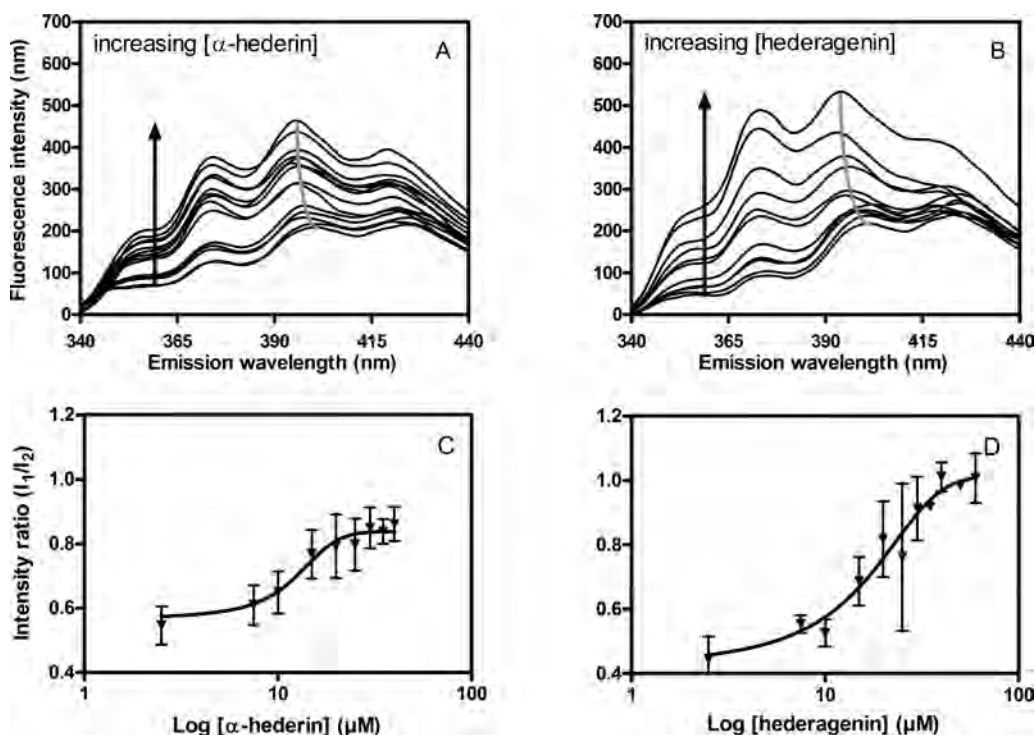
To characterize the calcein release, we adjusted the curve to a nonlinear regression that followed the equation

$$I(t) = I_S + \frac{I_0 - I_S}{1 + \exp\left(\frac{t - t_{1/2}}{\Delta t}\right)}$$

$I(t)$  is the fluorescence intensity caused by the release of calcein.  $I_S$  is the fluorescence when the release is maximized,  $I_0$  is the minimal fluorescence,  $t_{1/2}$  is the time when the release is 50% of the maximum ( $I_S$ ), and  $\Delta t$  is the characteristic time of the sigmoidal curve. The rate of release ( $\Delta p$ ) is the maximum of the first derivative function of  $I(t) \leftrightarrow d^2I(t)/dt^2 = 0$ .<sup>24</sup>

**AFM of Supported Planar Bilayers (SPBs).** SPBs were prepared on mica as previously described.<sup>37</sup> Briefly, 50  $\mu\text{L}$  of LUVs in 500  $\mu\text{M}$





**Figure 1.** Fluorescence emission spectra of DHE in aqueous solution (0.1% DMSO,  $\lambda_{\text{exc}} = 310 \text{ nm}$ ) (A, B). Increasing concentrations (arrow) of  $\alpha$ -hederin (A) and hederagenin (B) (from 0 to  $60 \mu\text{M}$ ) were used. The DHE concentration was set up at  $4 \mu\text{g}/\text{mL}$ . Fluorescence intensity ratio  $I_{375}/I_{395}$  with respect to  $\log_{10}$   $\alpha$ -hederin (C) and hederagenin (D) concentration is shown, and the inflection point was determined via a nonlinear regression (Hill function) of the data. The gray lines represent the blue shift of the second maxima.

DMPC/Chol (3:1 mol/mol) in buffer containing 20 mM  $\text{CaCl}_2$  was deposited onto freshly cleaved mica mounted on a Teflon disk. Samples were incubated at  $65^\circ\text{C}$  for 2 h in an oven preventing water evaporation. After this period, nonadsorbed liposomes and calcium were eliminated by gentle washing with buffer (10 mM Tris, 150 mM NaCl, pH 7.40).

Liquid AFM imaging was performed using a multimode microscope controlled by Nanoscope V electronics (Bruker AXS Corporation, Santa Barbara, CA) in contact mode (CMAFM). To perform AFM imaging, it was necessary to drift equilibrate and thermally stabilize the cantilever for no less than 30 min in the presence of buffer. To minimize the applied force on the sample, the set point was continuously adjusted during imaging. V-shaped  $\text{Si}_3\text{N}_4$  cantilevers (MLCT-AUNM, Veeco) with a nominal constant of  $0.01 \text{ N m}^{-1}$  were used. Images were acquired at a  $0^\circ$  scan angle at a scan rate of 2 Hz. All images were processed through commercial NanoScope Analysis software (Bruker AXS Corporation, Santa Barbara, CA).

For the 3D reconstruction of AFM sheets (Gwyddion 2.26, GNU [General Public License]), we corrected for horizontal scars and leveled the image by mean plane subtraction. We used the full  $z$  scale for representation, which is shown on the right side of each sheet. Three-dimensional reconstruction parameters were  $\varphi = 40^\circ$ ,  $\theta = -61^\circ$ , scale = 2.3, and value scale = 0.1.

Texture profiles of AFM raw data were made using the same processing methods as for 3D reconstruction. The texture profile was extracted from a straight line at  $y = 9.48 \mu\text{m}$  (red line, Figure 9A). We used this line because it passes through a small hole in the SPB that is present before the injection of  $\alpha$ -hederin, therefore indicating the thickness of the bilayer as  $\sim 4 \text{ nm}$ .

## RESULTS

**Formation of Mixed Micelles (Aggregates) between DHE and  $\alpha$ -Hederin or Hederagenin.** To characterize the interactions of saponin and triterpenic acid with sterols, we analyzed the effects of  $\alpha$ -hederin (Figure 1A,C) and hederagenin (Figure 1B,D) on DHE in aqueous solution. By adding  $\alpha$ -hederin

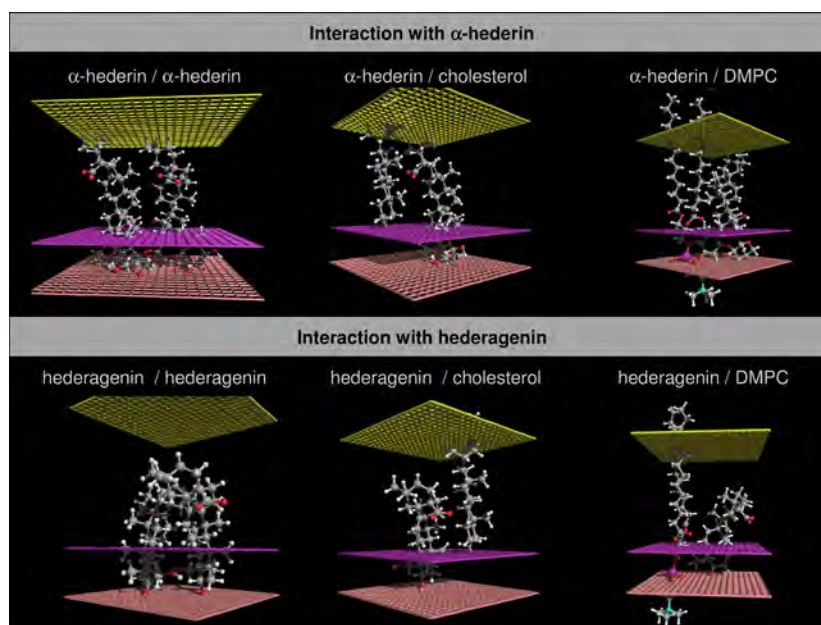
at increasing concentrations, we observed (i) a shift in the emission maxima from 402 to 396 nm (Figure 1A) and (ii) an increase in the intensity ratio between the monomeric peak (first maximum at 375 nm) and the structured emission (second and third maxima at around 395 and 424 nm) ( $I_{375}/I_{395}$  or  $I_{375}/I_{424}$ ) (Figure 1C). The blue shift could correspond to the formation of DHE/ $\alpha$ -hederin aggregates, as previously suggested.<sup>13</sup> The increase in the ratio between the monomeric peak and the structured emission reflects the separation of DHE molecules from their microcrystals and preferential interaction with saponin molecules.

Hederagenin was more efficient than  $\alpha$ -hederin regarding the blue shift of the structured peak (402 to 391 nm) (Figure 1B) and the increase in the intensity ratio (Figure 1D). Hederagenin would induce a more hydrophobic environment for DHE than  $\alpha$ -hederin most probably because of the lack of a sugar chain at C3.

When the intensity ratio was plotted against the logarithm of  $\alpha$ -hederin/hederagenin concentration (Figure 1C,D), we obtained a sigmoidal relation. For  $\alpha$ -hederin, we found an inflection point of  $12.33 \pm 3.21 \mu\text{M}$  that corresponded closely to its cmc value that was previously reported ( $13 \mu\text{M}$  in water).<sup>38</sup> For hederagenin, the inflection point was  $14.33 \pm 8.46 \mu\text{M}$ . To our knowledge, the cmc of hederagenin has not been reported in the literature, but asiatic acid, whose structure is only slightly different from that of hederagenin, possesses a cmc of  $15 \pm 2 \mu\text{M}$  (in PBS at pH 7.2).<sup>39</sup>

At a glance, these results suggest that  $\alpha$ -hederin and hederagenin are able to form mixed micelles (aggregates) in aqueous solution with sterols above critical concentrations of 12 and  $14 \mu\text{M}$ , respectively.

**Molecular Interaction with Lipids.** To gain information about the preferential orientation of  $\alpha$ -hederin/hederagenin in



**Figure 2.** Molecular modeling of complexes of  $\alpha$ -hederin and hederagenin with themselves, cholesterol, and DMPC in a lipid membrane. Three grids are representative of the different parts of the membrane: the yellow one represents the hydrophobic center of the membrane, the violet grid separates the hydrophobic core from the hydrophilic part, and the rose grid reflects the interfacial area separating the membrane from the aqueous environment.

membranes and their molecular interaction with DMPC/cholesterol, we used molecular modeling.

$\alpha$ -Hederin was inserted into the membrane by pointing its sugar moiety toward the outside of the membrane (Figure 2). This sugar moiety was placed in the hydrophilic part of the membrane. In contrast, the triterpenic part was located in the lipophilic portion of the membrane in the lipophilic portion of the membrane. When interacting with cholesterol,  $\alpha$ -hederin pointed its beta side toward the beta side of the cholesterol molecule. In contrast, when  $\alpha$ -hederin interacted with DMPC, its beta side points away from the phospholipid. A ternary complex composed of cholesterol,  $\alpha$ -hederin, and DMPC could therefore be possible. This is similar to what has been proposed for glycoalkaloids.<sup>14</sup>

Triterpenic acid hederagenin was less deeply inserted into the hydrophobic core than was the aglycone of its corresponding saponin. The sugar chain could therefore play an important role and force the saponin deep into the membrane by interacting with the hydrophilic heads of the surrounding molecules. The formation of a ternary complex cannot be excluded from hederagenin because it is bound in a different manner to cholesterol than to DMPC.

**Phase Separation of Sterols and Phospholipids in MLVs.** To investigate the potential of  $\alpha$ -hederin or hederagenin to induce phase separation in bilayers composed of cholesterol and DMPC, we used a FRET assay. Because DHE and DPH-PC partition like their nonfluorescent counterparts in membranes, cholesterol, and phospholipids, respectively,<sup>16,21</sup> a reduction in FRET efficiency reflects the local separation of phospholipids and cholesterol.

Figure 3 shows the FRET efficiency between DHE and DPH-PC ( $I_{430}/I_{371}$ ) with time (3 h) and increasing  $\alpha$ -hederin (A, C, E) or hederagenin (B, D, F) total lipid ratios. The FRET efficiency was between 2 and 3 in the control DMPC/Chol (3:1) MLVs and was stable over time.

The addition of  $\alpha$ -hederin induced a continuous decrease in the FRET efficiency with time and concentration (Figure 3A).

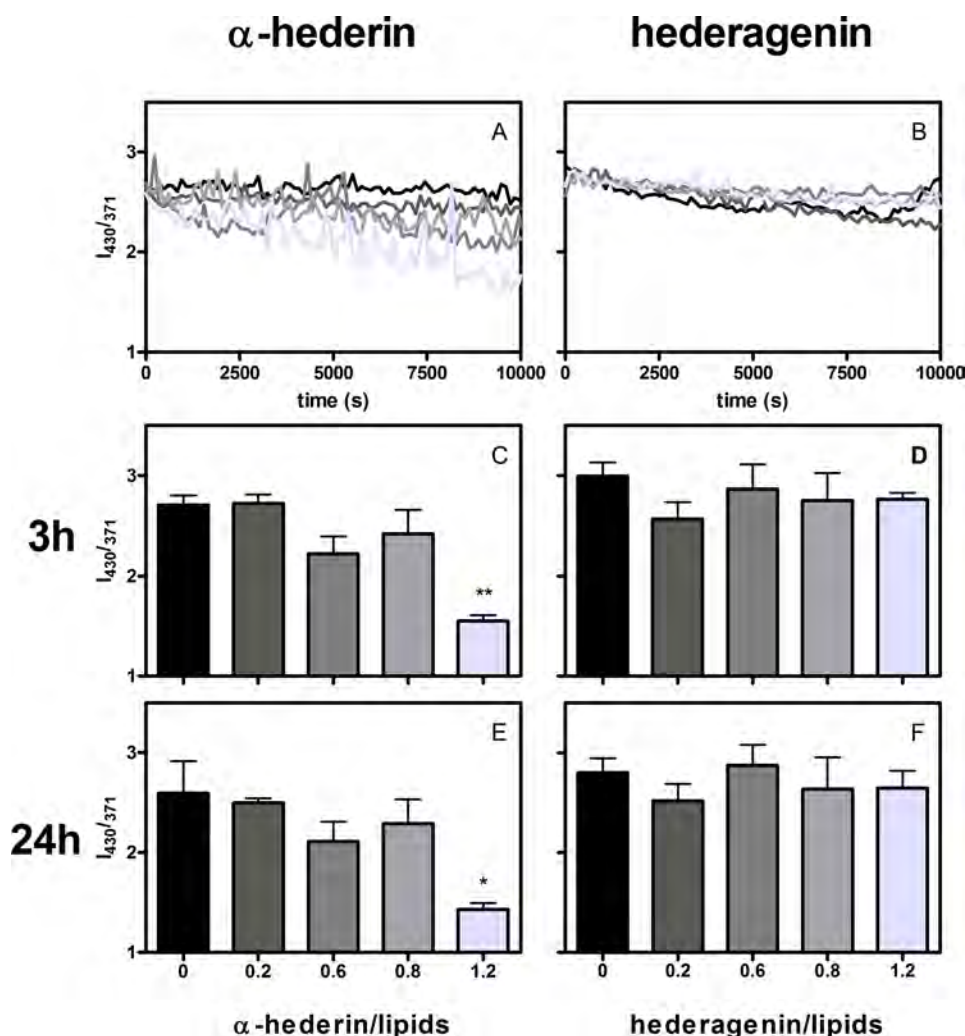
After 3 h of incubation, a significant decrease was observed at the highest  $\alpha$ -hederin/lipid ratio (1.2) (Figure 3C). Longer incubation periods (24 h) did not have any further effect (Figure 3E).

Conversely, hederagenin was not able to significantly reduce the FRET efficiency at 3, 24 (Figure 3D,F), or even 48 h (data not shown) regardless of the molar ratios of hederagenin/lipids used.

Accordingly, upon addition of  $\alpha$ -hederin, we observe an increase in the distance between sterols and phospholipids. This suggests a molecular reorganization of the bilayer or the extraction of a component from the membrane.<sup>16</sup>

**Visualization of Domain Formation in GUVs by Fluorescence Microscopy.** To visualize the formation of lipid domains, we used GUVs labeled with TR-DPPE (Figure 4A,C, red), (Figure 4B,D, yellow), and NBD-DPPE (Figure 4B,D, green). For the control (0.1% DMSO), no domain formation (A, B) was observed during 2 h 40 min. Also, at longer incubation periods DMSO did not induce any domain formation. In the presence of  $\alpha$ -hederin (10  $\mu$ M; Figure 4C,D), after 2 h both fluorescent lipids became concentrated into small spots around the vesicle (see arrow). Later, after 2 h 15 min, the small spots fused into a tubular network around the vesicle. At 2 h 20 min, parts of the membrane became deprived of TR-DPPE but still contained NBD-DPPE (Figure 4C,D, 2 h 20 min). At the same time, mainly TR-DPPE was accumulated on one or two poles of the vesicle, or it was concentrated in a belt around the vesicle. Finally at 2 h 40 min, a deformation of the vesicle into an oval form and the formation of crystalline-like structures around the vesicle were observed. The concentration of fluorescent lipids within specific domains was confirmed by octadecylrhodamine (R18), another fluorescent probe (data not shown).

To visualize the process in more detail, we recorded a movie of GUVs marked with TR-DPPE. The resolution is low, but important features are visible (Movie S.1). The movie shows that once domain formation becomes visible the process is relatively fast and needs only a few minutes to be completed. Again, we



**Figure 3.** Effect of  $\alpha$ -hederin (A, C, E) and hederagenin (B, D, F) on the fluorescence energy transfer efficiency between DHE and DPH-PC ( $I_{430}/I_{371}$ ) for the control (black) and increasing compound/lipid ratios (0.2, 0.6, 0.8, and 1.2 (increasingly brighter greys)) in MLVs composed of DMPC/Chol (3:1 mol/mol). The FRET efficiency is represented at 3 h of incubation (A, B) and at two selected time points: 3 h (C, D) and 24 h (E, F). The concentration of MLVs was set to  $50 \mu\text{M}$ . The experiments were performed at  $25^\circ\text{C}$ , and the curves represent three independent experiments. Statistical analysis: (*t* test) vs control, \* $p < 0.05$ , \*\* $p < 0.01$ .

observed the formation of a tubular network around the vesicle that collapsed and aggregated into several points (poles) on the vesicle.

Conversely to what was observed with  $\alpha$ -hederin, hederagenin ( $40 \mu\text{M}$ ) induced the formation of small, round domains enriched in fluorescent lipids that did not fuse into larger aggregates (Figure 4C). The first domains appeared after 1 to 2 h of incubation, but the phenomenon became important only after longer incubation periods (4–48 h) and at higher concentrations as compared to that of  $\alpha$ -hederin.

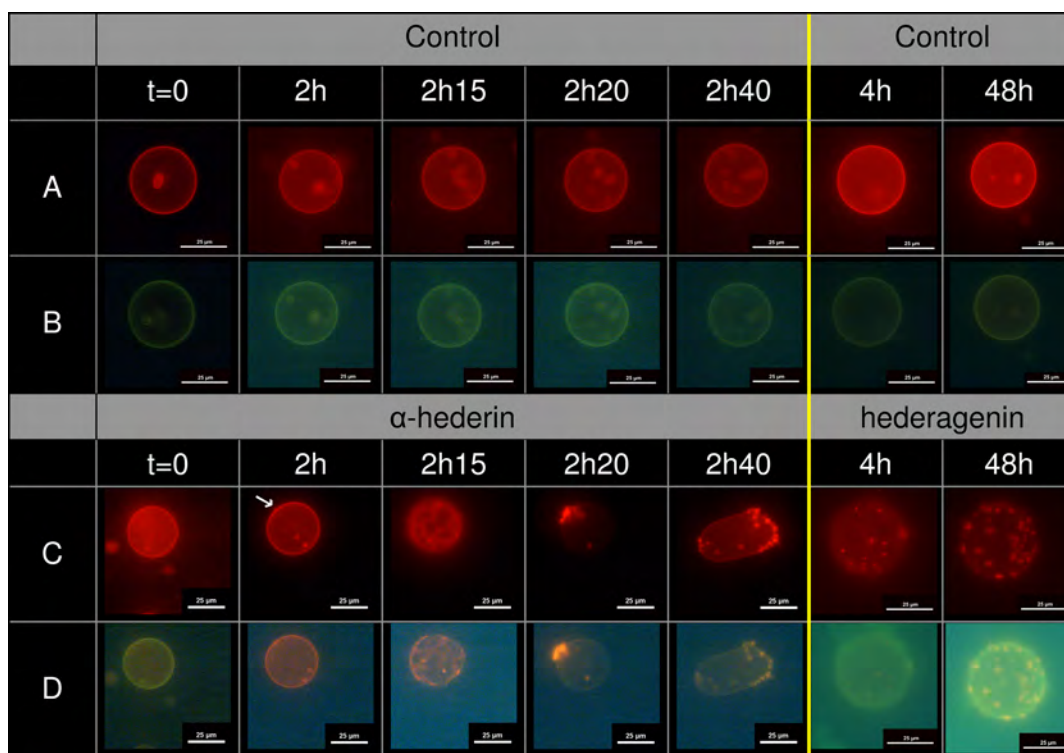
The formation of large and small domains with  $\alpha$ -hederin and hederagenin, respectively, has been shown *in silico* (Figure S1).

In addition to domain formation, we also observed vesiculation, budding, wrinkling, and pore formation when GUVs were incubated with  $\alpha$ -hederin. Representative pictures of GUVs accompanied by the quantification of these events are shown in Figure 5. Quantification pointed out that the most important feature observed on GUVs that have been incubated for 1 and 2 h with  $10 \mu\text{M}$   $\alpha$ -hederin was domain formation ( $54.4 \pm 13.3$  and  $65.7 \pm 12.9\%$ , respectively), followed by wrinkling and vesiculation or budding. At very short incubation times (a

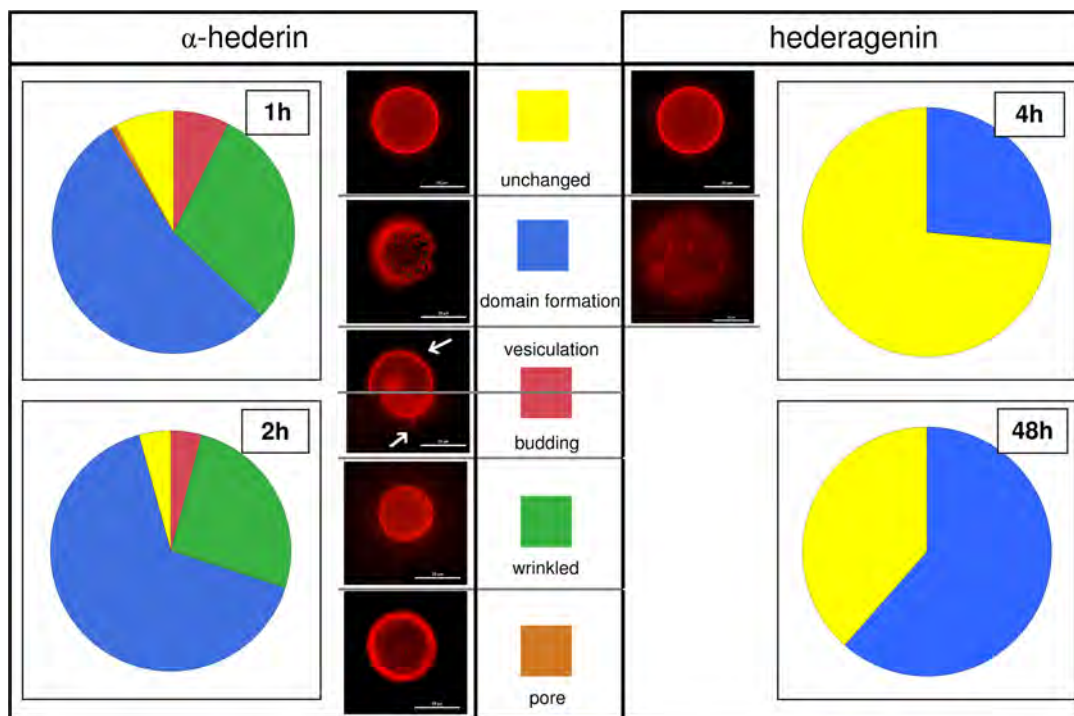
few seconds to  $\sim 15$  min), we observed the formation of smaller vesicles out of the mother vesicle (vesiculation). The formation of small buds was in this case followed by the fission of the membrane. At longer incubation times (1 to 2 h), buds remained connected through necks to the original GUV (budding) and no fission occurred. Only a very small population of GUVs showed macroscopic pore formation after 1 h (0.7%). With  $40 \mu\text{M}$  hederagenin, we observed  $26.6 \pm 1.8\%$  domain formation after 4 h of incubation and  $61.5 \pm 1.5\%$  after 48 h. Neither wrinkling, budding, nor pore formation was observed. At a glance, domain formation induced by  $\alpha$ -hederin was faster, domains were larger, and the concentration required to induce the process was less important as compared to the conditions for hederagenin.

**Characterization of Domain Formation by Confocal and Two-Photon Microscopy.** To characterize the domain formation induced by  $\alpha$ -hederin, we performed confocal microscopy of GUVs composed of DMPC/Chol (3:1 mol/mol) and labeled with TR-DPPE and NBD-DPPE (Figure 6A–C). Two-photon microscopy of GUVs composed of DMPC/DHE (3:1 mol/mol) and 0.1% TR-DPPE was used to assess the role of sterols in this process (Figure 6D,E). In control





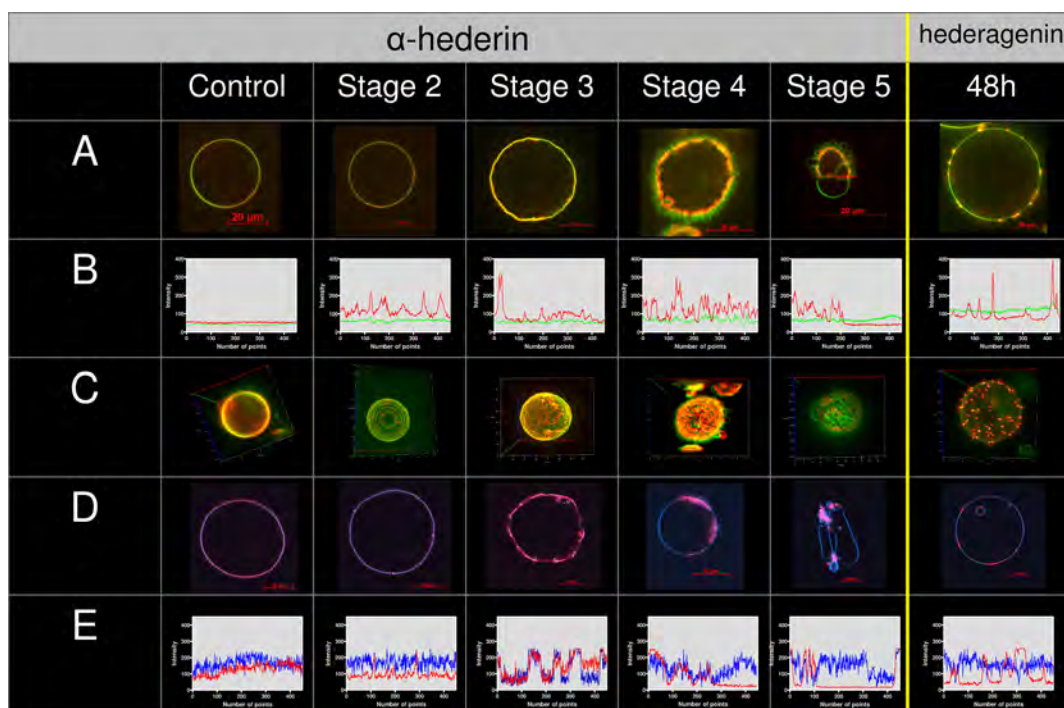
**Figure 4.** Induction of domain formation with  $10 \mu\text{M}$   $\alpha$ -hederin and  $40 \mu\text{M}$  hederagenin on GUV formed from DMPC/Chol (3:1) and marked by TR-DPPE and NBD-DPPE. The control was incubated with 0.1% (v/v) DMSO. Until 2 h 40 min, one GUV was followed and incubated with DMSO (A,B) and  $\alpha$ -hederin (C, D). At 4 and 48 h of incubation, pictures of representative GUVs incubated with DMSO (A, B) and hederagenin (C, D) are shown. Lines A and C correspond to the fluorescence of TR-DPPE (red), and lines B and D correspond to the fluorescence of TR-DPPE (red) and NBD-DPPE (green) simultaneously.



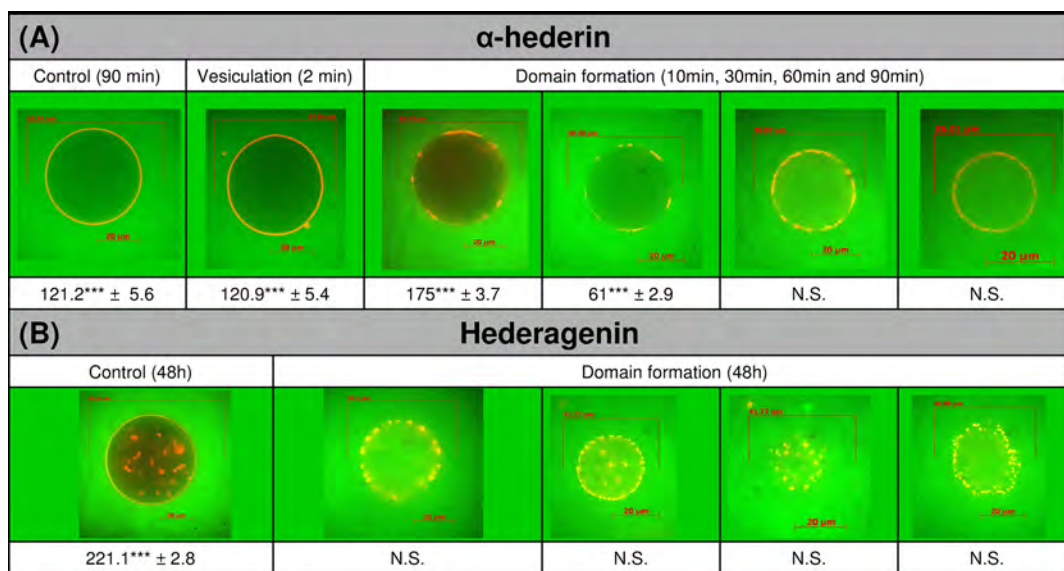
**Figure 5.** Representative pictures and percentages of GUVs composed of DMPC/Chol (3:1 mol/mol) incubated with  $10 \mu\text{M}$   $\alpha$ -hederin for 1 and 2 h or with  $40 \mu\text{M}$  hederagenin for 4 and 48 h and presenting different features (domain formation, vesiculation, budding, wrinkling, pore formation, or no change).

membranes composed of DMPC and cholesterol or DHE (3:1 mol/mol; Figure 6, control), we did not observe any visible

macroscopic phase separation. This is typical for binary mixtures of phospholipids and sterols<sup>40</sup> probably because of the fact that



**Figure 6.** (A–C) Confocal microscopy of domain formation induced by  $\alpha$ -hederin ( $10 \mu\text{M}$ ) and hederagenin ( $40 \mu\text{M}$ ) in GUVs formed from DMPC/Chol (3:1) containing 0.1% mol TR-DPPE (red) and NBD-DPPE (green). (D, E) Two-photon microscopy of GUVs composed of DMPC/DHE (3:1) and containing 0.1 mol% TR-DPPE. DHE is represented in blue, and TR-DPPE is represented in red. The controls were incubated with 0.1% DMSO. We took pictures of representative GUVs at different stages of phase separation. (A, D) Cross section at the axis of the vesicle. (B, E) Fluorescence intensity profile of the TR-DPPE (red), NBD-DPPE (green), and DHE (blue) vesicle contours from GUVs shown in A and D. (C) Three-dimensional reconstruction of all cross sections of GUVs shown in A.

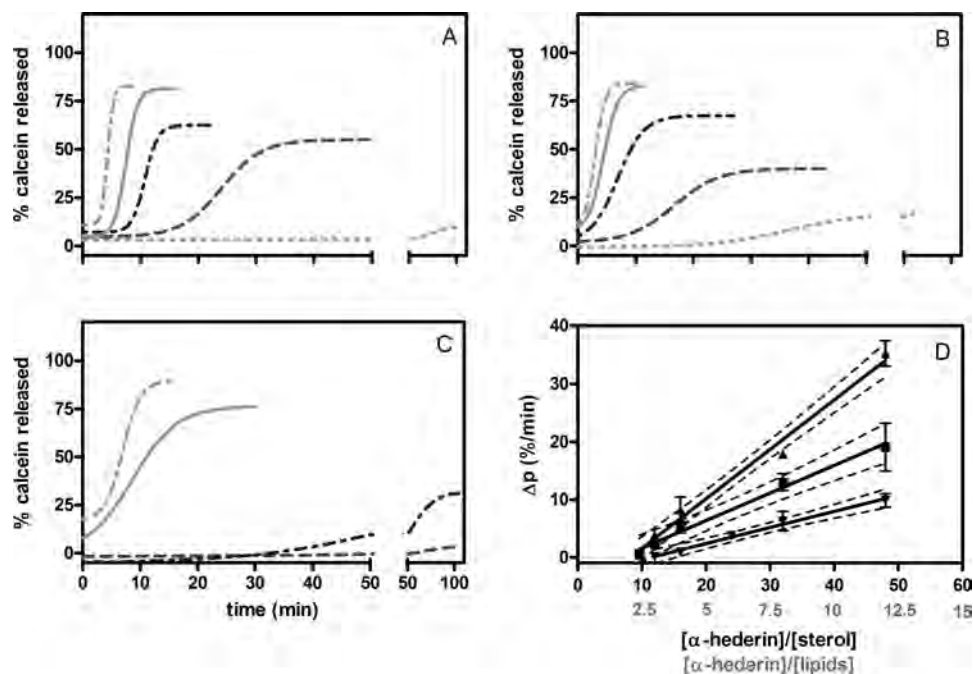


**Figure 7.** Permeation to FITC-dextran (4 kDa) of GUVs with  $10 \mu\text{M}$   $\alpha$ -hederin (A) at 2, 10, 30, 60, and 90 min or  $40 \mu\text{M}$  hederagenin (B) at 48 h. We show representative GUVs presenting different features such as domain formation or vesiculation. Controls were incubated with 0.1% DMSO. For each time point, the difference in normalized fluorescence between the inside and outside of the vesicle was quantified. Statistical analysis (*t* test) \*\*\*:  $p < 0.001$ . N.S. means no significant difference.

domains are in the nanometer range and are too small to be detectable.<sup>41</sup> For GUVs incubated with  $\alpha$ -hederin at  $10 \mu\text{M}$  (Figure 6,  $\alpha$ -hederin), the formation of new domains was observed. We confirmed a time dependency of the processes induced by the saponin as already observed in fluorescence microscopy. The initiation of small round-shaped domains (spots, stage 2) preceded the formation of wormlike aggregates

(stage 3) around the vesicles and the formation of a tubular network. These domains accumulated mainly TR-DPPE and DHE and to a lesser extent NBD-DPPE (stages 2 and 3; B, E). At the end of the process, the TR-DPPE/DHE-containing phase became more condensed and accumulated at one or two poles of the vesicle (stage 5). In parallel, the resting parts of the membrane became deprived of TR-DPPE (stages 4 and 5) but





**Figure 8.** Percentage of calcein release from LUV composed of DMPC/cholesterol (3:1) (A), DMPC/stigmasterol (3:1) (B), and DMPC/ergosterol (3:1) (C). The positive control (100% release) was 2% Triton X-100. LUV have been incubated at increasing  $\alpha$ -hederin/cholesterol ratios of 9.6 ( $\cdots$ ), 12 ( $-\cdot-\cdot-$ ), 16 ( $-\cdot-\cdot-$ ), 32 ( $-$ ), and 48 ( $-\cdot-\cdot-$ ) until a maximum release has been reached. The graphs show the curves obtained by fitting a one-phase exponential association function of one representative release assay by nonlinear regression. (D) Effect of increasing  $\alpha$ -hederin/sterol (black) or  $\alpha$ -hederin/lipid (gray) ratio on the maximum speed of calcein release (%/min,  $\Delta p$ ) for vesicles composed of DMPC/cholesterol ( $\blacktriangle$ ), DMPC/stigmasterol ( $\blacksquare$ ), or DMPC/ergosterol ( $\blacktriangledown$ ). Each value is the mean of triplicate measurements. The straight lines represent the linear fitting of the data, and the dotted line is the 95% confidence interval.

still contained DHE and NBD-DPPE. These parts of the membrane lost their rigidity, and the formation of small “blebs” (stage 4) preceded the formation of large protuberations and the loss of the spherical GUV shape. This phenomenon is more obvious in confocal/two-photon microscopy than in fluorescence microscopy where the formation of NBD-DPPE-containing blebs has not been observed. This might be due to the fact that the process is slower in confocal/two-photon microscopy sheets or because the axial resolution in confocal/two-photon microscopy is higher.

Domains induced by 40  $\mu$ M hederagenin after 48 h of incubation were mainly enriched in TR-DPPE (Figure 6, hederagenin) and to a smaller extent in NBD-DPPE. DHE did not accumulate in these domains contrary to what was observed with  $\alpha$ -hederin. Domains in DMPC/DHE vesicles were generally larger than in vesicles composed of DMPC/cholesterol.

At a glance,  $\alpha$ -hederin was able to concentrate DHE and TR-DPPE into domains that developed from small, round spots into wormlike aggregates before they were separated from the resting vesicles. NBD-DPPE was less accumulated in these spots. Hederagenin mostly accumulated TR-DPPE and to a lesser extent NBD-DPPE but not DHE into small persistent domains.

**Permeabilization of GUVs and LUVs.** To gain insight into the consequences of these effects on membrane permeability, we followed the permeation of GUVs to FITC-dextran (4 kDa) and calcein release from LUVs.

When GUVs were incubated with 10  $\mu$ M  $\alpha$ -hederin (Figure 7), permeation to FITC-dextran was not observed in GUVs presenting vesiculation (Figure 7, vesiculation). Moreover, GUVs presenting domain formation were not always permeabilized, suggesting that permeabilization was a graded process

(Figure 7, domain formation). Permeabilization was clearly time-dependent.

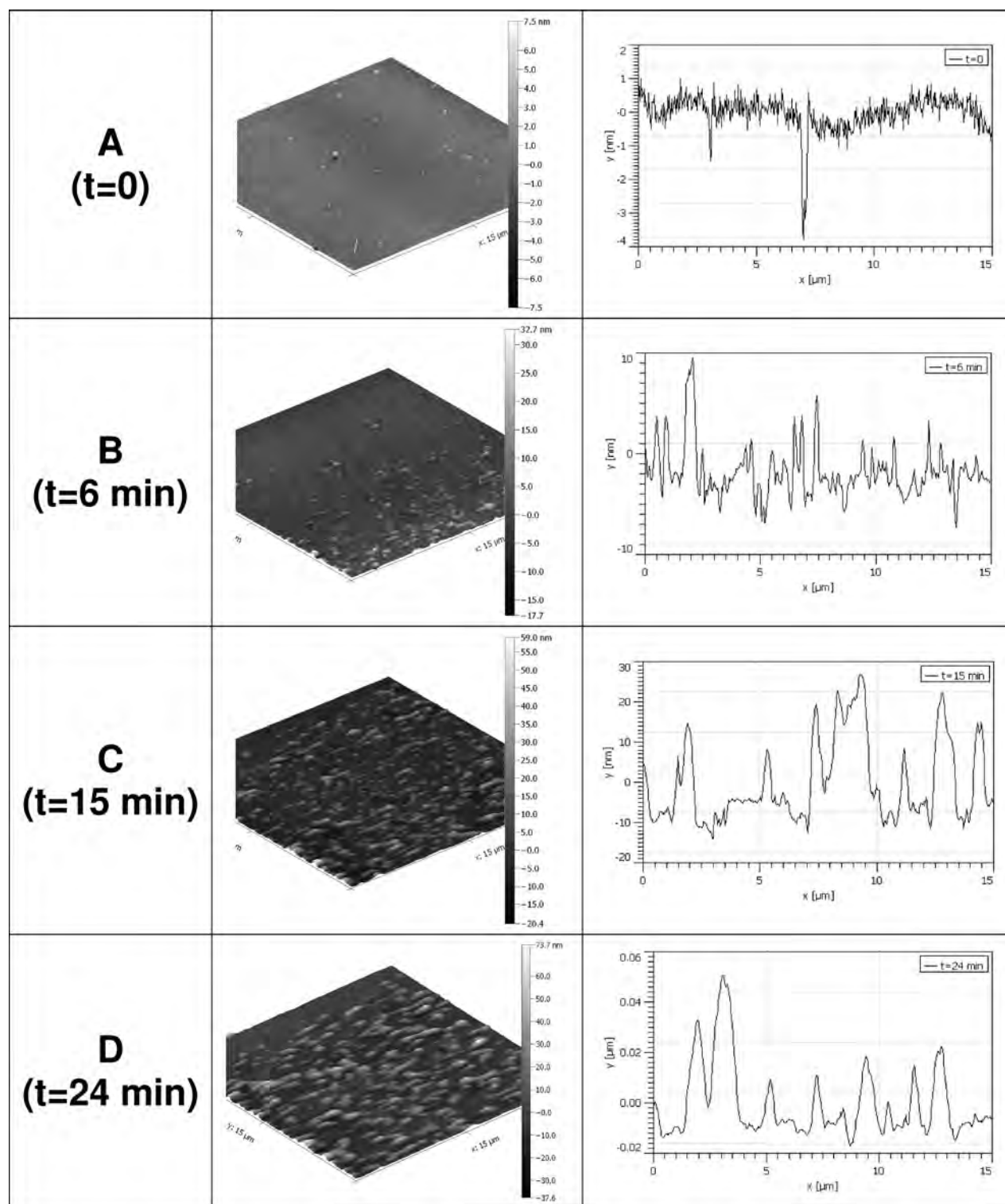
When GUVs were incubated with 40  $\mu$ M hederagenin for 48 h of incubation, permeation to FITC-dextran was observed only in vesicles presenting domain formation.

To investigate the kinetics of permeabilization and the importance of the membrane sterol, we prepared LUVs composed of DMPC and cholesterol (Figure 8A), stigmasterol (Figure 8B), or ergosterol (Figure 8C) in a fixed molar DMPC/sterol ratio at 3:1 and determined the ability of  $\alpha$ -hederin to induce membrane permeabilization. Figure 8A–C shows that regardless of the sterol type, the release of calcein followed a sigmoidal curve with increasing incubation time after an initial lag time. The lag time and the maximum release were dependent upon the  $\alpha$ -hederin/sterol ratio.

The slopes at the inflection point give insight into the importance of the sterol type on the rate of calcein release ( $\Delta p$ ) induced by  $\alpha$ -hederin (Figure 8D). These slope values were  $0.857 \pm 0.047$ ,  $0.478 \pm 0.056$ , and  $0.279 \pm 0.029$  for cholesterol, stigmasterol, and ergosterol, respectively.

Thus, the nature of the sterol composition of the liposomes is critical for membrane permeabilization induced by  $\alpha$ -hederin, with cholesterol allowing the fastest membrane permeabilization, followed by stigmasterol and ergosterol.

**Disruption of the Bilayer and Pore Formation in Supported Planar Bilayers.** Figures 9 and S2 show the effect of  $\alpha$ -hederin on DMPC/Chol (3:1 mol/mol) SPBs. The injection of 10  $\mu$ M  $\alpha$ -hederin did not have any effect on the membrane (data not shown). At 20  $\mu$ M (Figure S2), saponin induced the appearance of a new lower domain than the original bilayer and an increase in the covering of the mica surface (detailed description in the Supporting Information).



**Figure 9.** (Left column) 3D reconstruction of AFM raw data of SPB composed of DMPC/Chol (3:1 mol/mol). (Right column) Texture profiles corresponding to the red line in the first AFM sheet (positioned  $9.48 \mu\text{m}$  from the left edge). The red arrows indicate the holes induced by  $\alpha$ -hederin. The SPB was incubated with  $40 \mu\text{M}$   $\alpha$ -hederin for  $t = 0$  (A), 6 (B), 15 (C), and 24 min (D). The z-scale bar indicates the height difference between the highest and lowest values.

To understand better how  $\alpha$ -hederin interacts with SPB, we used a higher concentration of the molecule ( $40 \mu\text{M}$ , Figure 9). Figure 9A shows an SPB of DMPC/Chol (3:1 mol/mol) covering nearly 99% of the image, with features similar to those of SPB presented in Figure 9A. After the injection of  $\alpha$ -hederin to a final concentration of  $40 \mu\text{M}$  (Figure 9B–D), we observed the

appearance of small domains presenting increasing size and height. At the end of incubation (Figure 9D), the domains presented a wormlike shape, and the height of these domains was about 40–70 nm, reflecting a transformation of the bilayer structure (4 nm of height) into a new mesophase presenting a higher intrinsic curvature. The transformation of the bilayer into

a nonlamellar phase and the importance of cholesterol in this process was confirmed by  $^{31}\text{P}$  NMR on MLV (Figure S3). Parallel to the formation of domains, we observed an increasing number of holes in the bilayer (red arrows). These holes became larger with incubation time. However, we did not show a complete solubilization of the bilayer.

At a glance, we observed the formation of new domains in a concentration-dependent manner. At small concentrations, the covering of the mica surface is increased and lateral forces seem to decrease. At higher concentrations, the formation of larger holes and the accumulation of lipid material into wormlike aggregates is observed.

## DISCUSSION

Lipid phase separation has become an important concept in membrane organization. Cholesterol is one of the main lipids characterizing lipid domains and rafts. We previously showed that the interaction of cholesterol and  $\alpha$ -hederin would lead to the induction of increased transbilayer curvature in the membrane and toroidal pores.<sup>13</sup> In this work, we characterized the ability of  $\alpha$ -hederin to form lateral domains and induce phase separation in bilayer models (MLV, GUV, and SPB) composed of DMPC and cholesterol or DHE. In GUV and SPB, small lipid domains composed of phospholipids and sterols evolve into wormlike structures that are able to fuse into tubular aggregates. These tubules form a network around the GUV, which further collapses. These newly formed lipid aggregates accumulate preferentially at one or two poles of the vesicle. We highlighted the critical role of the saponin concentration as well as the importance of the presence of a sugar chain on the aglycone. With hederagenin, the domain formation is less marked, and higher concentrations and longer incubation periods are required to observe lipid domains. Moreover, domains induced by hederagenin are mainly composed of phospholipids and maintain a small round shape in DMPC/Chol membranes (at least after 48 h of incubation), in contrast to those observed with  $\alpha$ -hederin. Both molecules were able to induce the permeation of GUVs to dextran-FITC. In SPB, we observed in parallel to the formation of membrane domains the formation of holes in the membrane, which suggests that both processes are linked. We highlighted the importance of the membrane sterol in the kinetics of permeabilization of LUVs and showed that permeabilization is faster in liposomes containing cholesterol than in those containing stigmasterol or ergosterol.

Several mechanisms could be involved to explain the ability of  $\alpha$ -hederin and hederagenin to induce lipid phase separation. Phase separation in lamellar phases is mainly driven by an increase in the line tension ( $\lambda$ ) between domains and the surrounding phase<sup>40</sup> whereas repulsive electrostatic forces between domains and curvature tend to reduce it.<sup>42</sup> In a binary model composed of DMPC and cholesterol, nanoscopic phase separation below the resolution limit of an optical microscope is expected at room temperature (25 °C).<sup>16,17</sup> A mismatch between different intrinsic curvatures of  $L_o$  and  $L_d$  domains would create elastic interactions at phase boundaries that reduce line tension and so inhibit macroscopic phase separation.<sup>18</sup> Another critical parameter that opposes lipid phase separation is the entropy of lipid mixing. The lateral lipid distribution is dominated by the entropy of lipid mixing in the absence of preferred lipid interactions in a stationary system.<sup>43</sup> A high affinity of  $\alpha$ -hederin or hederagenin for one specific lipid component and the modulation of membrane curvature at phase boundaries are

probably enough to explain lipid phase separation despite the loss of entropy.

The formation of segregated domains by  $\alpha$ -hederin and hederagenin is followed by the disruption of the lamellar phase. This has been shown by AFM, where the results demonstrated a time-dependent increase in the grain size and height suggesting the accumulation of membrane material into these domains. The height of the newly formed wormlike structures largely overcomes the original bilayer thickness (from 4 to 40–70 nm), which agrees with the transformation of the bilayer into a nonbilayer mesophase. This confirms our previous  $^{31}\text{P}$  NMR data,<sup>13</sup> which showed the appearance of a hexagonal pattern with  $\alpha$ -hederin, in accordance with the highly curved tubular structures.<sup>44</sup> Hederagenin induced an isotropic pattern that could correspond to the small round domains observed.<sup>13</sup> The new structures present a higher intrinsic curvature than the original bilayer.<sup>44</sup> The increased membrane curvature in  $\alpha$ -hederin/lipid aggregates can be explained by the 3D molecular structure of the molecule.  $\alpha$ -Hederin is composed of two hydrophilic sugar units that point in one direction compared to its rigid triterpenic hydrophobic ring. The alignment of  $\alpha$ -hederin molecules in the membrane would therefore lead to positive curvature in one direction of the membrane plane, which would favor the formation of tubular wormlike aggregates.<sup>13</sup> Hederagenin, because of its sterol-like shape, should induce the formation of negatively curved structures.<sup>45</sup> The formation of preferentially inverted micelles has also been proposed for another pentacyclic triterpenic acid, ursolic acid.<sup>46</sup>

The molecular compositions of the newly formed aggregates are different for  $\alpha$ -hederin and hederagenin.  $\alpha$ -Hederin induced the aggregation of mainly TR-DPPE and DHE into domains, which reflects its affinity for sterols and phospholipids in the membrane. Molecular modeling shows that  $\alpha$ -hederin should be able to bind to phospholipids and cholesterol simultaneously and form a ternary complex. This is supported by data reported for another saponin,  $\alpha$ -tomatine.<sup>14</sup> Conversely, hederagenin did not induce the aggregation of DHE but mostly TR-DPPE and to a lesser extent NBD-DPPE in GUVs, which reflects an increased affinity for phospholipids. This might be due to the sterol-like molecular structure of triterpenic acid, which is responsible for the strong interaction with phospholipids.<sup>47</sup> In addition, two main observations support the preferential interaction of hederagenin with phospholipids. In membranes containing only DMPC, (i) the effect on membrane fluidity was more important than on those composed of DMPC/chol (3:1)<sup>13</sup> and (ii) hederagenin induced highly curved structures, conversely to  $\alpha$ -hederin, which required membrane cholesterol to be effective (Figure S3). At a glance, sterols would be less important for domain formation by hederagenin as compared to  $\alpha$ -hederin. The interaction of hederagenin with dehydroergosterol in aqueous solution does not exclude its higher affinity for phospholipids in membranes.

We also assessed in this work the importance of the sugar chain on the aglycone for phase separation and domain formation in MLVs and GUVs. In MLVs, hederagenin, lacking two sugar units, was not able to induce the phase separation of DHE and DPH-PC even after 48 h of incubation. This might be due to the fact that hederagenin preferentially interacts with phospholipids that are not adjacent to sterol molecules and thereby does not influence FRET efficiency. In other words, hederagenin preferentially interacts with the  $L_d$  phase. In GUVs, the rate of domain formation was largely reduced with hederagenin, and we did not observe the fusion of domains into wormlike structures,



conversely to what was observed with  $\alpha$ -hederin. The kinetics of domain formation and the shape of these domains would therefore be highly dependent on the sugar units: (i) An increase in the sugar length could favor the interaction with sterols in membranes, in accordance with the results obtained by two-photon microscopy. This might be due to an “umbrella” effect. The glycoside residues of the saponin would shield the nonpolar parts of sterols from water and thereby promote interaction between both molecules.<sup>48</sup> (ii) Hydrophilic sugar–sugar interactions between saponin molecules could increase the speed of domain formation in the membrane.<sup>14</sup>

Regarding the permeabilization mechanism induced by  $\alpha$ -hederin, we demonstrated that calcein release from LUV depended largely on the membrane sterol and the saponin/lipid ratio. At small ratios, we observed a lag time before calcein release was initiated. This lag time was efficiently reduced with increasing saponin concentrations, and once permeabilization was initiated, the rate of release was linearly dependent on the  $\alpha$ -hederin/lipid ratio and the sterol. The lag time might correspond to the time that was necessary to induce domain formation in GUV. In GUV, where the total lipid amount is very small compared to the amount of saponin, we first observed vesiculation and later a gradual permeation to FITC-dextran (4 kDa) at 10  $\mu$ M  $\alpha$ -hederin. Interestingly, we previously showed that  $\alpha$ -hederin at 40  $\mu$ M induced immediate membrane permeabilization and macroscopic pore formation but neither vesiculation nor phase separation.<sup>13</sup> The concentration of  $\alpha$ -hederin is hence critical for lipid phase separation, vesiculation, and membrane permeabilization. This could be related to the amphiphilic character of the saponin. Saponins are known to have surfactant activity, and they progressively reduce the surface tension of water in a concentration-dependent manner until their cmc is reached.<sup>38,49,50</sup> The cmc of  $\alpha$ -hederin is supposed to be close to 13  $\mu$ M,<sup>38</sup> which corresponds closely to the value that we obtained with DHE spectroscopy. Above this concentration, saponin should form aggregates or micelles in solution, as has been shown.<sup>50</sup>

On the basis of this data, we develop a new model for  $\alpha$ -hederin/membrane interaction that is dependent on the saponin concentration. Before any addition of  $\alpha$ -hederin, nanoscopic domains enriched in cholesterol would exist in the DMPC/Chol bilayer. Below the cmc (at 10  $\mu$ M),  $\alpha$ -hederin monomers would insert into the external monolayer and induce a rapid increase in the area difference between the outer and inner monolayers, which could lead to the induction of positive membrane curvature leading to vesiculation (budding followed by fission).<sup>44</sup> This has also been shown for other detergents with positive intrinsic molecular curvature.<sup>51</sup> At longer incubation periods, the cooperative association of  $\alpha$ -hederin, cholesterol, and DMPC could lead to the formation of curved domains in membrane whose size increases with time and that develop further into tubular or hexagonal aggregates. This aggregation is accelerated by the presence of a sugar chain at C3 and could be responsible for the development of membrane defects (as seen by AFM) and gradual permeabilization of the membrane. Above the cmc (at 40  $\mu$ M), micelles and other types of amphiphilic aggregates could be formed in aqueous solution, as demonstrated with other saponins.<sup>50</sup> When micelles would interact with membranes, they could directly deliver an increased local concentration of  $\alpha$ -hederin molecules to the membrane surface and therefore favor the direct formation of macroscopic pores, which could explain why  $\alpha$ -hederin permeabilizes the GUVs quasi-instantaneously at

40  $\mu$ M but needs more than 1 h at 10  $\mu$ M.<sup>13</sup> This agrees with the data recently reported for glycyrrhizin.<sup>11</sup>

Moving on to the effect of the aglycone, hederagenin induced no budding at 40  $\mu$ M. The induction of negative curvature into the external monolayer would be in accordance with this result. Membrane permeabilization and domain formation were observed after 48 h in GUV, where phase separation was ongoing. The aggregation of phospholipids into domains could promote the formation of membrane defects and permeabilization.<sup>5,52</sup> It is not clear if the interaction of hederagenin with the membrane depends on the formation of hederagenin-aggregates/micelles in the solution. Low concentrations of hederagenin did not show any effect on membranes. It might be possible that only aggregates of triterpenic acids have an effect on the membrane, as has been suggested for madecassic and asiatic acid.<sup>53</sup>

The possible biological effects of the proposed membrane interactions are numerous. It might be possible that the proposed permeabilization mechanism is responsible for hemolysis and cancer cell lysis by some triterpenic acids and saponins, a process that would strongly depend upon the concentration and the membrane sterol.<sup>54</sup> Additionally,  $\alpha$ -hederin may also show activity in fungi or plants because it permeabilized membranes composed of ergosterol and stigmasterol.

Regarding the effects on phase separation, it has been shown in biological membranes that the lateral organization of cholesterol influences membrane protein and drug activity. This has become a subject of great interest.<sup>55</sup> The specific interaction of some saponins with cholesterol led to the effect on lipid rafts and the induction of the extrinsic apoptotic pathway.<sup>9,10</sup> The accumulation of  $\alpha$ -hederin/hederagenin in the cellular membrane could lead to the unspecific activation of membrane proteins localized in rafts.

The model we established could be helpful in synthesizing new triterpenoids that are able to induce phase separation or domain formation. Regarding the role of the 3D shape of saponins, the presence or the orientation of sugar moieties could be critical to the rational design of those compounds.<sup>56</sup>

## ■ ASSOCIATED CONTENT

### 📄 Supporting Information

Materials and methods and results. A movie showing domain formation in a GUV marked by TR-DPPE. This material is available free of charge via the Internet at <http://pubs.acs.org>.

## ■ AUTHOR INFORMATION

### Corresponding Author

\*E-mail: [marie-paule.mingeot@uclouvain.be](mailto:marie-paule.mingeot@uclouvain.be).

### Notes

The authors declare no competing financial interest.

## ■ ACKNOWLEDGMENTS

Special thanks to Henri Burhin and Christian Bailly for suggestions about polymers and providing the PDMS for the electroformation chamber. We are also grateful for the 31P NMR experiments performed by Cécile S. Le Duff. This work has been funded by the FNRS (Fonds National de la Recherche Scientifique, contract nos. 3.4.588.10 and 3.4.578.12) and the Université Catholique de Louvain Bourse du Patrimoine. Two-photon microscopy was financed by the FNRS, the Region of Brussels, and the UCL.

## REFERENCES

- (1) Lingwood, D.; Simons, K. Lipid rafts as a membrane-organizing principle. *Science* **2010**, *327*, 46–50.
- (2) Simons, K.; Vaz, W. L. Model systems, lipid rafts, and cell membranes. *Annu. Rev. Biophys. Biomol. Struct.* **2004**, *33*, 269–295.
- (3) de Kruijff, B. Lipid polymorphism and biomembrane function. *Curr. Opin. Chem. Biol.* **1997**, *1*, 564–569.
- (4) Luzzati, V. Biological significance of lipid polymorphism: the cubic phases. *Curr. Opin. Struct. Biol.* **1997**, *7*, 661–668.
- (5) Hallock, K. J.; Lee, D. K.; Ramamoorthy, A. MSI-78, an analogue of the magainin antimicrobial peptides, disrupts lipid bilayer structure via positive curvature strain. *Biophys. J.* **2003**, *84*, 3052–3060.
- (6) Almgren, M. Mixed micelles and other structures in the solubilization of bilayer lipid membranes by surfactants. *Biochim. Biophys. Acta* **2000**, *1508*, 146–163.
- (7) Lohner, K.; Staudegger, E.; Prenner, E. J.; Lewis, R. N.; Kriechbaum, M.; Degovics, G.; McElhaney, R. N. Effect of staphylococcal delta-lysin on the thermotropic phase behavior and vesicle morphology of dimyristoylphosphatidylcholine lipid bilayer model membranes. Differential scanning calorimetric, <sup>31</sup>P nuclear magnetic resonance and Fourier transform infrared spectroscopic, and X-ray diffraction studies. *Biochemistry* **1999**, *38*, 16514–16528.
- (8) Bangham, A. D.; Horne, R. W.; Glauert, A. M.; Dingle, J. T.; LUCY, J. A. Action of saponin on biological cell membranes. *Nature* **1962**, *196*, 952–955.
- (9) Yi, J. S.; Choo, H. J.; Cho, B. R.; Kim, H. M.; Kim, Y. N.; Ham, Y. M.; Ko, Y. G. Ginsenoside Rh2 induces ligand-independent Fas activation via lipid raft disruption. *Biochem. Biophys. Res. Commun.* **2009**, *385*, 154–159.
- (10) Xu, Z. X.; Ding, T.; Haridas, V.; Connolly, F.; Gutterman, J. U. Avicin D, a plant triterpenoid, induces cell apoptosis by recruitment of Fas and downstream signaling molecules into lipid rafts. *PLoS One* **2009**, *4*, e8532.
- (11) Sakamoto, S.; Nakahara, H.; Uto, T.; Shoyama, Y.; Shibata, O. Investigation of interfacial behavior of glycyrrhizin with a lipid raft model via a Langmuir monolayer study. *Biochim. Biophys. Acta* **2013**, *1828*, 1271–1283.
- (12) Bayer, M.; Proksch, P.; Felsner, I.; Brenden, H.; Kohne, Z.; Walli, R.; Duong, T. N.; Gotz, C.; Krutmann, J.; Grether-Beck, S. Photoprotection against UVAR: effective triterpenoids require a lipid raft stabilizing chemical structure. *Exp. Dermatol.* **2011**, *20*, 955–958.
- (13) Lorent, J.; Le Duff, C. S.; Quetin-Leclercq, J.; Mingeot-Leclercq, M. P. Induction of highly curved structures in relation to membrane permeabilization and budding by the triterpenoid saponins, alpha- and delta-Hederin. *J. Biol. Chem.* **2013**, *288*, 14000–14017.
- (14) Keukens, E. A.; de Vrije, T.; van den, B. C.; de Waard, P.; Plasman, H. H.; Thiel, F.; Chupin, V.; Jongen, W. M.; de Kruijff, B. Molecular basis of glycoalkaloid induced membrane disruption. *Biochim. Biophys. Acta* **1995**, *1240*, 216–228.
- (15) Elias, P. M.; Goerke, J.; Friend, D. S.; Brown, B. E. Freeze-fracture identification of sterol-digtonin complexes in cell and liposome membranes. *J. Cell Biol.* **1978**, *78*, 577–596.
- (16) Loura, L. M.; Fedorov, A.; Prieto, M. Fluid-fluid membrane microheterogeneity: a fluorescence resonance energy transfer study. *Biophys. J.* **2001**, *80*, 776–788.
- (17) de Almeida, R. F.; Loura, L. M.; Prieto, M. Membrane lipid domains and rafts: current applications of fluorescence lifetime spectroscopy and imaging. *Chem. Phys. Lipids* **2009**, *157*, 61–77.
- (18) Meinhardt, S.; Vink, R. L.; Schmid, F. Monolayer curvature stabilizes nanoscale raft domains in mixed lipid bilayers. *Proc. Natl. Acad. Sci. U.S.A.* **2013**, *110*, 4476–4481.
- (19) van Meer, G. Cellular lipidomics. *EMBO J.* **2005**, *24*, 3159–3165.
- (20) Stine, K. J.; Hercules, R. K.; Duff, J. D.; Walker, B. W. Interaction of the glycoalkaloid tomatine with DMPC and sterol monolayers studied by surface pressure measurements and Brewster angle microscopy. *J. Phys. Chem. B* **2006**, *110*, 22220–22229.
- (21) Wustner, D. Fluorescent sterols as tools in membrane biophysics and cell biology. *Chem. Phys. Lipids* **2007**, *146*, 1–25.
- (22) Juhasz, J.; Davis, J. H.; Sharom, F. J. Fluorescent probe partitioning in giant unilamellar vesicles of 'lipid raft' mixtures. *Biochem. J.* **2010**, *430*, 415–423.
- (23) Garvik, O.; Benediktson, P.; Simonsen, A. C.; Ipsen, J. H.; Wustner, D. The fluorescent cholesterol analog dehydroergosterol induces liquid-ordered domains in model membranes. *Chem. Phys. Lipids* **2009**, *159*, 114–118.
- (24) Loura, L. M.; Prieto, M. Dehydroergosterol structural organization in aqueous medium and in a model system of membranes. *Biophys. J.* **1997**, *72*, 2226–2236.
- (25) Cheng, K. H.; Virtanen, J.; Somerharju, P. Fluorescence studies of dehydroergosterol in phosphatidylethanolamine/phosphatidylcholine bilayers. *Biophys. J.* **1999**, *77*, 3108–3119.
- (26) Schroeder, F.; Barenholz, Y.; Gratton, E.; Thompson, T. E. A fluorescence study of dehydroergosterol in phosphatidylcholine bilayer vesicles. *Biochemistry* **1987**, *26*, 2441–2448.
- (27) Lins, L.; Thomas-Soumarmon, A.; Pillot, T.; Vandekerckhove, J.; Rosseneu, M.; Brasseur, R. Molecular determinants of the interaction between the C-terminal domain of Alzheimer's beta-amyloid peptide and apolipoprotein E alpha-helices. *J. Neurochem.* **1999**, *73*, 758–769.
- (28) Brasseur, R. TAMMO: Theoretical Analysis of Membrane Molecular Organization. In *Molecular Description of Biological Membrane Components by Computer-Aided Conformational Analysis*; Brasseur, R., Ed.; CRC Press: Boca Raton, FL, 1990.
- (29) Deleu, M.; Lorent, J.; Lins, L.; Brasseur, R.; Braun, N.; El Kirat, K.; Nylander, T.; Dufrene, Y. F.; Mingeot-Leclercq, M. P. Effects of surfactin on membrane models displaying lipid phase separation. *Biochim. Biophys. Acta* **2013**, *1828*, 801–815.
- (30) Bartlett, G. R. Citation classic - phosphorus assay in column chromatography. *Current Contents/Life Sciences* **1985**, *16*.
- (31) Loura, L. M.; Fernandes, F.; Prieto, M. Membrane microheterogeneity: Forster resonance energy transfer characterization of lateral membrane domains. *Eur. Biophys. J.* **2010**, *39*, 589–607.
- (32) Parker, A.; Miles, K.; Cheng, K. H.; Huang, J. Lateral distribution of cholesterol in dioleoylphosphatidylcholine lipid bilayers: cholesterol-phospholipid interactions at high cholesterol limit. *Biophys. J.* **2004**, *86*, 1532–1544.
- (33) Angelova, M. I.; Soléau, S.; Méléard, Ph.; Faucon, J. F.; Bothorel, P. Preparation of giant vesicles by external AC electric fields. Kinetics and applications. *Prog. Colloid Polym. Sci.* **1992**, *89*, 127–131.
- (34) Dodes Traian, M. M.; Gonzalez Flecha, F. L.; Levi, V. Imaging lipid lateral organization in membranes with C-laurdan in a confocal microscope. *J. Lipid Res.* **2012**, *53*, 609–616.
- (35) Bagatolli, L. A.; Gratton, E. Two-photon fluorescence microscopy observation of shape changes at the phase transition in phospholipid giant unilamellar vesicles. *Biophys. J.* **1999**, *77*, 2090–2101.
- (36) Weinstein, J. N.; Yoshikami, S.; Henkart, P.; Blumenthal, R.; Hagsins, W. A. Liposome-cell interaction: transfer and intracellular release of a trapped fluorescent marker. *Science* **1977**, *195*, 489–492.
- (37) Domenech, O.; Francius, G.; Tulkens, P. M.; Van Bambeke, F.; Dufrene, Y.; Mingeot-Leclercq, M. P. Interactions of oritavancin, a new lipoglycopeptide derived from vancomycin, with phospholipid bilayers: Effect on membrane permeability and nanoscale lipid membrane organization. *Biochim. Biophys. Acta* **2009**, *1788*, 1832–1840.
- (38) Bottger, S.; Hofmann, K.; Melzig, M. F. Saponins can perturb biologic membranes and reduce the surface tension of aqueous solutions: a correlation? *Bioorg. Med. Chem.* **2012**, *20*, 2822–2828.
- (39) Rafat, M.; Fong, K. W.; Goldsipe, A.; Stephenson, B. C.; Coradetti, S. T.; Sambandan, T. G.; Sinskey, A. J.; Rha, C. Association (micellization) and partitioning of aglycon triterpenoids. *J. Colloid Interface Sci.* **2008**, *325*, 324–330.
- (40) Veatch, S. L.; Keller, S. L. Separation of liquid phases in giant vesicles of ternary mixtures of phospholipids and cholesterol. *Biophys. J.* **2003**, *85*, 3074–3083.
- (41) Heberle, F. A.; Wu, J.; Goh, S. L.; Petruzielo, R. S.; Feigenson, G. W. Comparison of three ternary lipid bilayer mixtures: FRET and ESR reveal nanodomains. *Biophys. J.* **2010**, *99*, 3309–3318.

(42) Sriram, I.; Singhana, B.; Lee, T. R.; Schwartz, D. K. Line tension and line activity in mixed monolayers composed of aliphatic and terphenyl-containing surfactants. *Langmuir* **2012**, *28*, 16294–16299.

(43) Tian, A.; Baumgart, T. Sorting of lipids and proteins in membrane curvature gradients. *Biophys. J.* **2009**, *96*, 2676–2688.

(44) Zimmerberg, J.; Kozlov, M. M. How proteins produce cellular membrane curvature. *Nat. Rev. Mol. Cell Biol.* **2006**, *7*, 9–19.

(45) Chen, Z.; Rand, R. P. The influence of cholesterol on phospholipid membrane curvature and bending elasticity. *Biophys. J.* **1997**, *73*, 267–276.

(46) Prades, J.; Vogler, O.; Alemany, R.; Gomez-Florit, M.; Funari, S. S.; Ruiz-Gutierrez, V.; Barcelo, F. Plant pentacyclic triterpenic acids as modulators of lipid membrane physical properties. *Biochim. Biophys. Acta* **2011**, *1808*, 752–760.

(47) Mannock, D. A.; Lewis, R. N.; McMullen, T. P.; McElhaney, R. N. The effect of variations in phospholipid and sterol structure on the nature of lipid-sterol interactions in lipid bilayer model membranes. *Chem. Phys. Lipids* **2010**, *163*, 403–448.

(48) Huang, J.; Feigenson, G. W. A microscopic interaction model of maximum solubility of cholesterol in lipid bilayers. *Biophys. J.* **1999**, *76*, 2142–2157.

(49) Romussi, G.; Cafaggi, S.; Bignardi, G. Hemolytic action and surface activity of triterpene saponins from *Anchusa officinalis* L. Part 21: On the constituents of Boraginaceae. *Pharmazie* **1980**, *35*, 498–499.

(50) Mitra, S.; Dungan, S. R. Micellar properties of quillaja saponin O.1. Effects of temperature, salt, and pH on solution properties. *J. Agric. Food Chem.* **1997**, *45*, 1587–1595.

(51) Staneva, G.; Seigneuret, M.; Koumanov, K.; Trugnan, G.; Angelova, M. I. Detergents induce raft-like domains budding and fission from giant unilamellar heterogeneous vesicles: a direct microscopy observation. *Chem. Phys. Lipids* **2005**, *136*, 55–66.

(52) Correia, R. F.; Viseu, M. I.; Prazeres, T. J.; Martinho, J. M. Spontaneous vesicles, disks, threadlike and spherical micelles found in the solubilization of DMPC liposomes by the detergent DTAC. *J. Colloid Interface Sci.* **2012**, *379*, 56–63.

(53) Stephenson, B. C.; Goldsipe, A.; Blankschtein, D. Molecular dynamics simulation and thermodynamic modeling of the self-assembly of the triterpenoids asiatic acid and madecassic acid in aqueous solution. *J. Phys. Chem. B* **2008**, *112*, 2357–2371.

(54) Gauthier, C.; Legault, J.; Girard-Lalancette, K.; Mshvildadze, V.; Pichette, A. Haemolytic activity, cytotoxicity and membrane cell permeabilization of semi-synthetic and natural lupane- and oleanane-type saponins. *Bioorg. Med. Chem.* **2009**, *17*, 2002–2008.

(55) George, K. S.; Wu, S. Lipid raft: a floating island of death or survival. *Toxicol. Appl. Pharmacol.* **2012**, *259*, 311–319.

(56) Chwalek, M.; Lalun, N.; Bobichon, H.; Ple, K.; Voutquenne-Nazabadioko, L. Structure-activity relationships of some hederagenin diglycosides: haemolysis, cytotoxicity and apoptosis induction. *Biochim. Biophys. Acta* **2006**, *1760*, 1418–1427.



## **Supporting information**

### **Material and methods**

#### **Big layer method**

The method is based on the construction of a grid of 600 x 600 molecules and its minimization by a Monte Carlo procedure<sup>1</sup> using the interaction matrix (molecular modeling, main text), taking the molar ratios account. Graphically, each molecule type was represented by a colored point and all the points were represented on the grid. This allowed to visualize preferential interactions and phase separation between the molecules studied.

#### **AFM of supported planar bilayers (SPB)**

(see main text)

#### **Characterization of the new lipid phase by <sup>31</sup>P-NMR of MLVs**

MLVs (30 mg of total lipid in Tris-HCl at pH 7.4) were prepared according to the freeze-thawing method. Because <sup>31</sup>P-NMR spectroscopy requires high amounts of products, we avoided solubility problem by inserting  $\alpha$ -hederin and hederagenin during the lipid film formation. 0.3 ml of D<sub>2</sub>O was added for deuterium lock to 2.5 ml of samples. This sample was placed in a 10 mm Wilmad 575-pp NMR tube which rotated at 20 ppm in the NMR spectrometer. NMR spectra were acquired on a Bruker Avance DRX500 spectrometer operating at 500.13 MHz for <sup>1</sup>H (202.47MHz for <sup>31</sup>P) and equipped with a 10 mm Bruker Broadband Observe probe. The temperature in the probe was regulated at 37°C or 60°C for the duration of the experiments. All

$^{31}\text{P}$  spectra were referenced to the  $^{31}\text{P}$  peak from an 85% solution of phosphoric acid  $\text{H}_3\text{PO}_4$  measured at  $25^\circ\text{C}$  set at 0.0 ppm. One-dimensional  $^1\text{H}$  spectra were recorded prior to  $^{31}\text{P}$  experiments to ensure the best field homogeneity was attained for each sample. 114688 points and an acquisition time of 0.7 s using power-gated Waltz16  $^1\text{H}$  decoupling were used and 26000 scans per  $^{31}\text{P}$  experiment with a sweepwidth of 83.1kHz were acquired with a delay of 1.5s between scans. The signal was Fourier transformed using an exponential multiplication function with a line broadening of 50Hz and zero-filled to a final spectral resolution of 0.6Hz per point.

### **Fluorescence microscopy of GUVs (movie)**

A movie showing domain formation in a GUV marked by TR-DPPE was recorded (movie S1). Speed is accelerated 4 times (one second in the movie represents 4 real seconds) and contrast was slightly enhanced.

## **Results**

### *Simulation of domain formation*

After establishing the most probable interaction conformers by molecular modeling (see main text), we wanted to know how  $\alpha$ -hederin and hederagenin would partition laterally into a membrane composed of DMPC and cholesterol and if they would be able to induce a phase separation. For this purpose, we took benefit from Monte-Carlo simulations which simulated monolayers of different compositions. In monolayers containing 25% cholesterol, cholesterol domains were evidenced (Fig. S1A). This is in agreement with domains observed in Langmuir

monolayers composed of DMPC and cholesterol<sup>2</sup>. By adding  $\alpha$ -hederin, we observed a sequestration of cholesterol molecules into larger domains (Fig. S1B).  $\alpha$ -Hederin was located between cholesterol and DMPC molecules and “forced” the cholesterol molecules together.

Conversely, hederagenin induced the formation of smaller domains than  $\alpha$ -hederin (Fig. S1C).



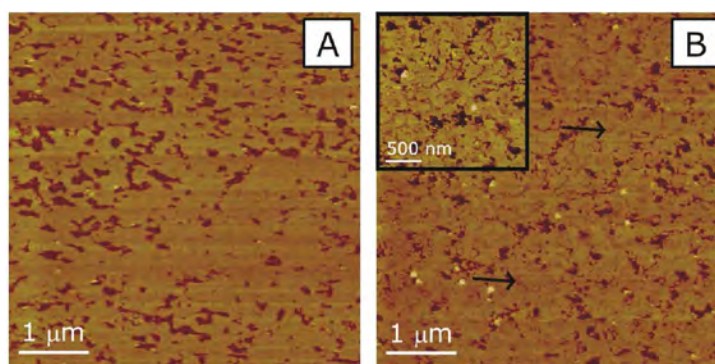
**Figure S1.** Figure caption. Monolayer grid of 200X200 molecules calculated by the Big Layer Method. Each pixel represents a molecule. Red: DMPC molecules; green: cholesterol molecules; white:  $\alpha$  hederin molecules and yellow : hederagenin molecules. (A) DMPC/Cholesterol at a molar ratio of 0.75:0.25, (B) DMPC/Cholesterol/ $\alpha$ -hederin at 0.67:0.23:0.1, (C) DMPC/Cholesterol/Hederagenin at 0.67:0.23:0.1.

#### Formation of a new domain with $\alpha$ -hederin

Prior to the injection of the molecule, SPBs were characterized in the presence of 1 % of DMSO showing no significant modification of the SPB due to the presence of the DMSO (Fig. S2A). We observed a flat SPB covering 85% of the surface with a step height of  $5.2 \pm 0.4$  nm and a roughness ( $R_a$ ) mean value of 0.3 nm.



After injection of  $\alpha$ -hederin to a final concentration of 20  $\mu$ M (Fig. S2B), the appearance of several structures that protrude  $6.5 \pm 1.5$  nm from the top of the SPB surface was clearly seen. The SPB covered 95 % of the image with a step height of  $4.3 \pm 0.6$  nm and  $R_a$  mean value of 0.2 nm. Interestingly, after the injection of  $\alpha$ -hederin, a lower domain appeared on the SPB surface as shown in the inset image (Fig. S2B). This domain was  $0.61 \pm 0.11$  nm lower than the top of the SPB. Furthermore the decrease in the thickness of the bilayer together with the increase in the covering of the mica surface suggest that  $\alpha$ -hederin interacts with the SPB decreasing lateral forces between lipid molecules.



**Figure S2.** Figure caption. (A) SPB of DMPC/Chol (3:1, mol/mol) in presence of 1% DMSO; B) the same SPB 30 min after injection of  $\alpha$ -hederin to a final concentration of 20  $\mu$ M. Inset, zoom image from (B). Z-scale bar was 20 nm.

### Transformation of the bilayer into non-lamellar phases

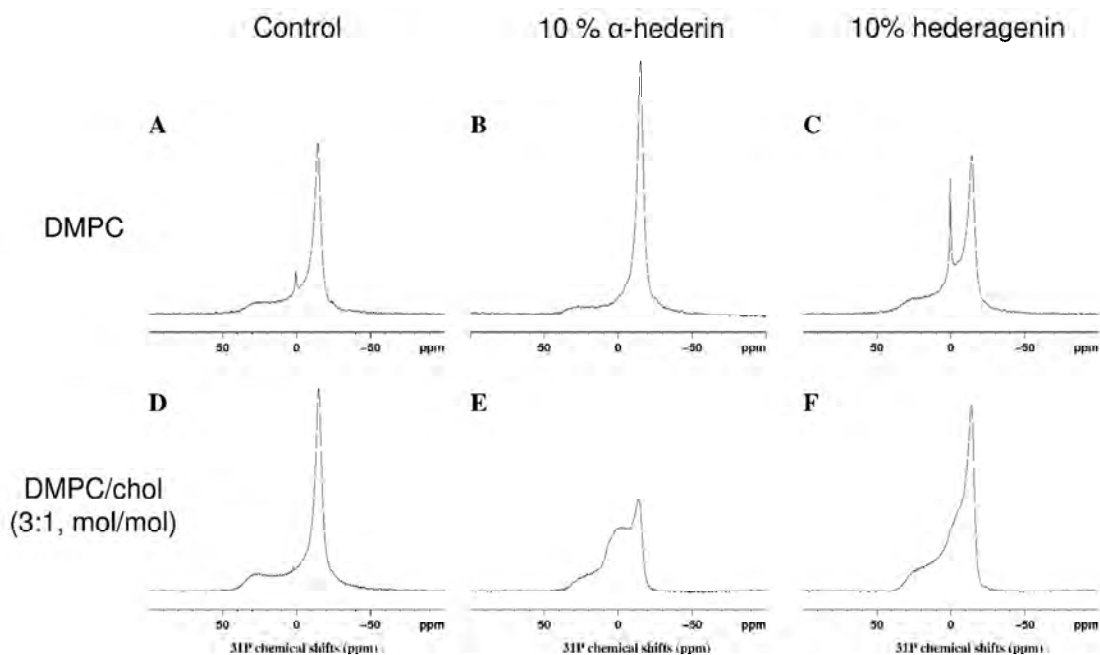
We performed  $^{31}\text{P}$ -NMR spectroscopy on MLVs to confirm the disruption of the bilayer and the formation of new lipid structures which we observed by AFM on SPB.

The controls show a typical bilayer signal with a high field peak and a low field shoulder (Fig. S3A,D).

In MLVs composed of only DMPC,  $\alpha$ -hederin did not modify the bilayer pattern (Fig. S3B). The chemical shift anisotropy was not significantly changed ( $42.5 \pm 1$  ppm to  $44 \pm 1$  ppm). Conversely, hederagenin induced a sharp isotropic peak at 0 ppm, meaning that hederagenin is able to form lipid structures with DMPC presenting isotropic motion (Fig. S3C). Isotropic motion is typical for structure of a size less than  $100 \text{ nm}^3$ . The chemical shift anisotropy was slightly reduced to  $39.5 \pm 1$  ppm reflecting the presence of structures with higher mobility or diffusibility.

In the presence of membrane cholesterol,  $\alpha$ -hederin becomes very effective in disrupting the bilayer signal (Fig. S3E). A new broad peak around 0 ppm is formed. This means that also phospholipids are present in the newly formed structures. The chemical shift anisotropy is efficiently reduced from  $39 \pm 1$  ppm to  $34.5 \pm 1$  ppm. Hederagenin only slightly modified the bilayer pattern (Fig. S3F) and the chemical shift anisotropy ( $36.5 \pm 1$  ppm).

At a glance, we show that  $\alpha$ -hederin only disrupts the bilayer in the presence of cholesterol and induced the formation of new phospholipid aggregates. Conversely, for hederagenin, the presence of cholesterol seems to inhibit the formation of new lipid aggregates presenting isotropic motion.



**Figure S3.** Figure caption :  $^{31}\text{P}$ -NMR spectra performed at  $25^\circ\text{C}$  on MLV composed of DMPC (A,B,C) or DMPC/chol (D,E,F). Spectra of control vesicles are shown in A and D. Spectra of vesicles containing 10% (%mol) of  $\alpha$ -hederin are shown in B and E and hederagenin in C and F.

#### Reference List

- (1) Deleu, M.; Lorent, J.; Lins, L.; Brasseur, R.; Braun, N.; El Kirat, K.; Nylander, T.; Dufrene, Y. F.; Mingeot-Leclercq, M. P. Effects of surfactin on membrane models displaying lipid phase separation. *Biochim.Biophys.Acta* **2013**, *1828*, 801-815.
- (2) Seul, M.; Sammon, M. J. Competing interactions and domain-shape instabilities in a monomolecular film at an air-water interface. *Phys.Rev.Lett.* **1990**, *64*, 1903-1906.
- (3) Schanck, A.; Deleers, M.  $^{31}\text{P}$  NMR study of the parameters influencing the formation of non-bilayer phases in model membrane. *Biochem.Biophys.Res.Commun.* **1993**, *195*, 654-658.